


Article

Mixed-Integer Distributed Ant Colony Optimization of Dump Load Allocation with Improved Islanded Microgrid Load Flow

Maen Z. Kreishan  and Ahmed F. Zobaa * 

Electronic and Electrical Engineering Department, Brunel University London, Uxbridge UB8 3PH, UK

* Correspondence: azobaa@ieee.org

Abstract: Dump load (DL) utilization at low demand hours in highly penetrated islanded microgrid is of great importance to offer voltage and frequency regulation. Additionally, load flow (LF) convergence is vital to optimize the working states of the DL allocation problem. Hence, more analysis is necessary to highlight the significance of DL in power regulation while observing the influence of LF on solution accuracy. This article proposes two LF techniques derived from backward/forward sweep (BFS), viz., general BFS (GBFS) and improved special BFS (SBFS-II). The latter is based on global voltage shared between generating units, while the former has a more general approach by considering generating bus's local voltage. The optimal sizing and sitting of DL with optimum droop sets are determined using the mixed-integer distributed ant colony optimization (MIDACO) with the two new LF methods. The optimization problem was formulated to minimize voltage and frequency deviations as well as power losses. The problem was validated on IEEE 69- and 118-bus systems and compared with established metaheuristics. Results show that DL allocation using MIDACO with SBFS-II and GBFS has improved the solution speed and accuracy, respectively. Furthermore, the enhanced voltage and frequency results highlight DL as an efficient power management solution.

Keywords: load flow; backward/forward sweep; dump load; droop control; islanded microgrid; ant colony optimization; multi-objective optimization



Citation: Kreishan, M.Z.; Zobaa, A.F. Mixed-Integer Distributed Ant Colony Optimization of Dump Load Allocation with Improved Islanded Microgrid Load Flow. *Energies* **2023**, *16*, 213. <https://doi.org/10.3390/en16010213>

Academic Editor: Mohamed Benbouzid

Received: 11 November 2022
Revised: 15 December 2022
Accepted: 21 December 2022
Published: 25 December 2022



Copyright: © 2022 by the authors. Licensee MDPI, Basel, Switzerland. This article is an open access article distributed under the terms and conditions of the Creative Commons Attribution (CC BY) license (<https://creativecommons.org/licenses/by/4.0/>).

1. Introduction

Adequate microgrid (MG) stability and reliability are fundamental for an overall resilient smart grid operation. The significance of reliable MG operation is vital in accommodating the shift toward decentralized power generation with an abundance of scattered renewable resources. To that end, optimization studies are necessary to strike a balance between running costs, renewable energy utilization, and autonomous MG stability and reliability. Autonomous MG operation and analysis, also known as islanded MG (IMG), is often an area for debate in the literature [1]. Moreover, international standards for successful operation of IMG necessitate maintaining voltage and frequency ($V - f$) levels within acceptable limits [2]. Hence, most IMG opted for the low-cost, decentralized, and reliable droop-control strategy [3]. Subsequently, autonomous networks with droop control are often referred to as droop-controlled IMG (DCIMG).

However, in highly penetrated DCIMG, the issue of $V - f$ regulation becomes a challenge, especially during off-peak hours, owing to the large power mismatch at low load hours. Different energy management systems (EMS) have been proposed to address power mismatch issues in DCIMG, such as demand response programs [4], energy storage systems (ESS) [5], and electric vehicles (EV) smart charging [6]. Nonetheless, during off-peak hours, such EMS solutions are not yet ready to handle large power mismatches in highly penetrated renewable based DCIMG due to cost [7] and coordination [8] issues. Consider a scenario where variable renewable generation is high and continues for two consecutive below-peak load cycles. The surplus power would have to be stored in any available battery ESS (BESS). Subsequently, if this high generation/demand mismatch

situation continues, the storage solutions would require replacement to absorb the surplus power in the system. This situation is costly and inefficient, especially for isolated and remote microgrids where cost is a significant factor. Consequently, a good solution would be to dump the excess power performing useful work such as heating and pumping applications. The use of DL in heating and pumping applications is beyond the scope of this article and requires work in an independent study. Nevertheless, the study presented in this article aims to highlight DL as a viable and cost-effective solution during off-peak hours' control for highly penetrated DCIMGs. Therefore, these EMS should handle small power mismatch as an auxiliary response during peak demand hours while employing dump loads (DL) to absorb excess generation as the primary response at low-demand hours.

Utilization of DL in synchronous and asynchronous generator-side $V - f$ regulation was achieved by means of electronic load controllers (ELC) for hydro and wind power generation disciplines [9,10]. Similarly, DLs were utilized in heating and pumping applications to enhance supply quality by means of power management and $V - f$ control [11,12]. Nevertheless, few studies have addressed the use of DL as an EMS solution in DCIMG framework [13,14]. On the contrary, the studies [15–21] have tackled economic, environmental, and technical objectives in the optimal allocation and operation of DCIMG with particular interest in DG and ESS. The allocation of ESS was utilized in DCIMG to minimize total MG cost in [15] and emissions in [16]. Similarly, the sizing and siting of DG units were optimized to maximize net energy exports [17], minimize energy losses [18], and maximize stability [19]. Additionally, the optimal droop settings were determined to minimize fuel costs [20] and maximize loadability [21]. Despite the various contributions made by DG and ESS studies, the authors of [15–21] did not account for $V - f$ regulation during off-peak hours. Therefore, neglecting the efficiency issues with existing storage-based EMS to handle large power mismatch [13].

To overcome EMS efficiency problems in handling large power mismatches, a DL-based EMS was proposed in [13]. The objective of this study was to minimize $V - f$ deviations during the low load hours by allocating DL to consume excess generation in heating applications [13]. However, the work presented in [13] did not account for MG power losses due to DL allocation, nor did it consider the droop setting of DG units. Moreover, the load flow (LF) method adopted, direct BFS (DBFS), suffered from convergence issues, while the run time of the utilized optimization technique, non-dominated sorting genetic algorithm (NSGA-II), was not practical for real-time application. One major concern for metaheuristics applied to real-time non-convex mixed-integer non-linear problems (MINLPs) is the calculation time and convergence speed. Various swarm and evolutionary stochastic techniques have been implemented in DCIMG optimization problems [13–21]. Most of these methods are based on the famous genetic algorithm (GA) and particle swarm optimization (PSO), as well as their expansion for MINLP multi-objective optimization. Further developments in metaheuristics are undergoing to achieve more efficient algorithms with a good balance between exploration and exploitation as well as convergence capabilities. A discrete metaheuristic method derived from the behaviour of real ants as they look for food is known as ant colony optimization (ACO) [22]. Subsequently, these discrete ACO techniques were further expanded to continuous domains [23] and multi-objective ACO (MOACO) [24]. The proposed method in this article, on the other hand, is formed using the extended ACO for mixed-integer domains (ACOMi) [25] as mingled with the oracle penalty method (OPM) for constraint handling [26]. The main difference between MOACO and the proposed method is the enhanced search effort for solutions on the Pareto front using the utopia-nadir balance technique [27]. The main advantage of the proposed optimization technique, MIDACO, against other acclaimed metaheuristics is the speed and accuracy for many-objective optimization problems [28,29].

Conversely, the availability of robust and efficient LF analysis tools for DCIMG is of great importance to predicting the behavior of such systems. Thus, better planning and modeling of IMG in optimization studies are possible. Conventional load flow techniques, such as Newton–Raphson (N-R), fast decoupled, and Gauss–Seidel (G-S) suffer from

limitations when applied to ill-conditioned distribution networks [30,31]. According to the notable work of Shirmohammadi et al. [30], Jacobean-based load flow methods are not suitable for distribution networks. This is due to the high R/X ratio of distribution networks, which enfeebles the Jacobean diagonal predominance, causing singularity in the matrix [32]. This issue was further proven in [33], where BFS convergence was more immune than Jacobean-based methods if applied to distribution networks with variations in R/X ratio and generation/loading levels. To overcome Jacobean methods' shortfalls in distribution networks, BFS was recommended by [30] for distribution systems that are topologically radial or weakly meshed in nature. Nonetheless, conventional BFS techniques are not suitable to be applied directly to IMGs. This is attributed to the absence of a slack bus and the variable frequency nature of islanded networks. Subsequently, the available LF techniques for DCIMGs can be broadly classified into Jacobean and derivative-free techniques. As in [34], different modes of operations for DG units were incorporated in an LF technique derived from the Newton trust region. Likewise, the N-R method was modified to solve the LF problem for DCIMG in [35–37]. The aim of the latter studies was to expand the Jacobean matrix to incorporate the variable voltage and frequency of DCIMGs. Despite the robustness of the N-R methods suggested in [35–37], they do not take advantage of the topological nature of microgrids, which is radial. Additionally, the Jacobian matrix is known to be computationally expensive and requires more memory for larger systems with additional Jacobean matrices [38,39].

A derivative-free LF based on the famous BFS method was proposed in [40]. This method, called DBFS, offers a faster and more stable LF solution to radial and weakly meshed DCIMG compared to the Jacobean-based methods. Moreover, a modified BFS (MBFS) method was suggested by [41] to take local voltage measurements by droop-controlled units into account. Likewise, ref. [42] proposed a nested BFS (NBFS) that is based on the MBFS method with an improved convergence rate. The use of swarm intelligence techniques in the power flow problem of IMGs was proposed in different studies for isolated AC [43,44] and DC microgrids [45]. The aim of the studies in [43,44] was to find the optimal droop sets that achieve the best active and reactive power sharing for units in DCIMG. Likewise, as in [45], the optimal resistive droop value was determined considering uncertainty in generation and demand to achieve optimal current sharing between DG units. Nonetheless, the limited convergence and calculation burden of methods mentioned heretofore acts as a limitation in optimization problems for ill-conditioned and radial power networks. Such ill-conditioning as caused by higher generation/demand mismatches and lower reactive droop sets would limit the boundary conditions for optimization variables. Moreover, the application of optimization methods in load flow techniques in [43–45] was problem-specific, assuming certain loading conditions of the system. Moreover, their computational burden is huge and would lead to slower calculation speeds. This would limit their application to small networks or DC microgrids. As a result, they could not be generalized for optimization problems that require thousands of function evaluations of converged LF solutions in highly penetrated DCIMGs.

Conversely, a robust LF method, called special BFS (SBFS), was utilized with the state-of-the-art MIDACO algorithm to improve the stability of highly penetrated IMG [14]. The non-dominated solution for DL allocation problem was selected by MIDACO based on load flow provided by a global voltage update mechanism. Nonetheless, the LF solution attained by SBFS assumes full communication between the units and thus did not account for local voltage measurements for DGs. Moreover, the two internal loops of SBFS add an extra calculation burden to the optimization technique implemented. This might lead to slower calculation times for larger systems or problems with stochastic uncertainty modeling.

In this article, the many-objectives problem for DL allocation in highly penetrated DCIMG is handled via two proposed LF methods, viz., SBFS-II and GBFS. The aim of this article is to further improve the DL size and location, as well as the optimal droop set for optimal DG dispatch as attained by MIDACO with SBFS [14]. Accordingly, SBFS-II, being the first proposed method herein, is based on SBFS, with only one loop to enhance the

convergence rate compared to the original SBFS and its counterpart DBFS. The second method, on the other hand, i.e., general BFS (GBFS), employs dynamic damping factors and a correction vector to enhance convergence. Thus, GBFS offers a more accurate representation of LF in DCIMG with and without communication between units. Furthermore, the GBFS method offers enhanced convergence compared to its counterparts MBFS and NBFS by employing voltage error damping and reactive power correction. The two LF methods were combined with MIDACO to minimize four objectives, namely voltage and frequency deviations, as well as active and reactive power losses. This is attained by the optimal sizing and sitting of DL, as well as optimal DG droop selection. Moreover, to shed more light on the sensitivity of the DL allocation problem to the LF method used within the optimization technique. As previously described, there are two main methods for power flow of DCIMG, viz., derivative-free and Jacobean-based. However, the proposed LF techniques herein were utilized for optimization problem with a vast number of function evaluations. Therefore, BFS-based load flow methods were sought over Jacobean-based methods to minimize the calculation time and enhance the convergence at high power mismatches and lower droop values. This is of paramount importance to enable further renewable energy integration and optimization studies that require simpler, highly convergent, and current-based techniques for radial distribution systems [46]. A comparison between the current state of the art on load flow analysis tools for DCIMG that are based on BFS for islanded systems is given in Table 1.

Table 1. Comparison between BFS-based load-flow methods for islanded systems.

LF Method	DG Voltage Update	Number of Loops	Damping Factors	Reactive Power Correction	No DG Communication Required	Reference
DBFS	Global	3	No	No	No	[40]
MBFS	Local	3	No	No	Yes	[41]
NBFS	Local	3	Static	No	Yes	[42]
SBFS	Global	2	No	No	No	[14]
SBFS-II	Global	1	No	No	No	-
GBFS	Local	1	Dynamic	Yes	Yes	-

This article is arranged as follows: in Section 1, an introduction of the DL allocation problem in DCIMG is presented. In Section 2, droop control, special BFS, and the proposed two load flow methods are explained. In Section 3, the proposed optimization technique, MIDACO, is elucidated. In Section 4, the optimization problems for GBFS and DL allocation are expanded. Lastly, in Sections 5 and 6, the optimization problem results and conclusions are presented, respectively. Additionally, to enhance the readability of this article, a list of all symbols used herein is given in Table A1 in Appendix A. Similarly, to highlight the main steps and concepts covered by the dump load allocation problem in DCIMG during off-peak hours, a generic flow chart for the overall proposed methodology is illustrated in Figure 1.

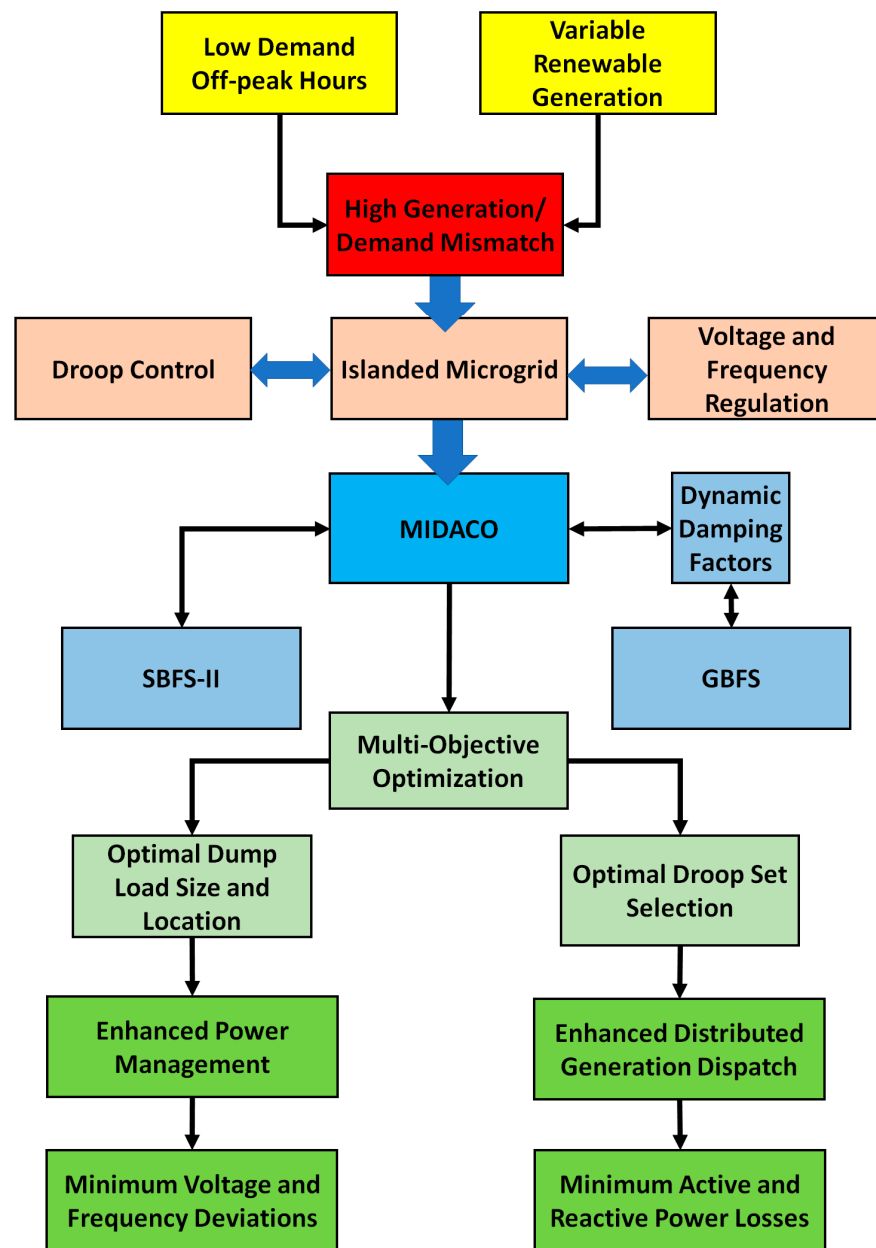


Figure 1. Generic flow chart for dump load allocation in DCIMG.

2. Droop Control and Load-Flow Analysis in Islanded Microgrid

In this section, the proposed methodology for droop control and load-flow analysis in islanded microgrid is explained in detail.

2.1. Droop Control and Special Backward\Forward Sweep (SBFS) Load Flow Method

In an IMG, the comprehensive control strategy is usually implemented in three levels, viz., primary, secondary, and tertiary. For primary control, it is undertaken in a matter of milliseconds via the droop control, whereas secondary control allows for the restoration of $V - f$ reference points without changing the droop coefficients. Lastly, the tertiary control level is responsible for the optimal operation of an IMG by utilizing the MG central controller (MGCC) to form the complete hierarchal energy management system of an IMG [47,48]. Generation units in an IMG are usually modeled as inverter-based DGs (IBDGs) with a power electronics interface to enable $V - f$ droop control. This is necessary

to enable the contribution of each dispatchable unit to the total load in the MG. The IBDG primary droop control relations are depicted in the $P - f$ and $Q - V$ curves of Figure 2.

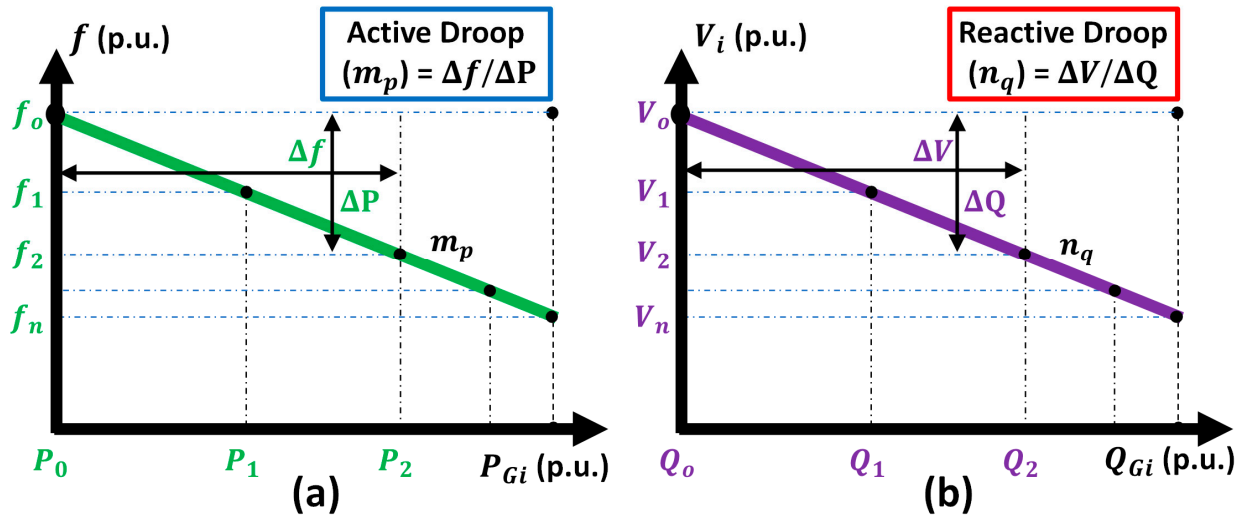


Figure 2. Droop curves for generating units: (a) $P - f$ droop, (b) $Q - V$ droop.

Each DG contributes to load variation in proportion to its respective droop coefficient, where a DG with a lower droop will contribute more to demand change. Moreover, in an overgeneration situation, the DG unit's reactive and active power output will decrease to suppress the rise in bus voltage and system frequency, respectively. This is often referred to as the $P - f$ and $Q - V$ droop relations of an IBDG. From Figure 2, the active and reactive power updates from each DG happen in a stepwise process until power mismatch is satisfied at a droop bus. Note that the deviation in DG power with respect to load change in the first step is much larger than that of the second step, and so on. Thus, the influence of steps succeeding the first one at steady state is often negligible. Subsequently, Equations (1) and (2) relating the $P - f$ and $Q - V$ droops, respectively, are embedded within the IBDG control system. This shall enable DGs to follow load variations based on their respective droop coefficients as required by IEEE std.1547.7 [49],

$$f - f_0 = m_{pi} (P_{Gi} - P_{Gi0}), \quad (1)$$

$$|V_i| - |V_0| = n_{qi} (Q_{Gi} - Q_{Gi0}), \quad (2)$$

where f and f_0 are the operational and reference frequency, respectively; $|V_i|$ and $|V_0|$ are the operational and reference voltage at bus i , respectively; P_{Gi} and P_{Gi0} are the operational and reference generated active power at bus i , respectively; Q_{Gi} and Q_{Gi0} are the operational and reference generated reactive power at bus i , respectively; and n_{qi} and m_{pi} are bus i 's reactive and active droop coefficients, respectively.

The model used to represent the generating units herein is that of the IBDG, while the droop coefficients of the base case (i.e., No DL case) for this study are given in Table 2 [14]. On the other hand, load modeling for this study follows the exponential load model presented in [50]. The use of static exponential load models is widely sufficient to model static load components and approximate the dynamic components [50]. For the sake of brevity, the constant power model was adopted throughout all simulations of this study; this can be achieved by setting all load coefficients to zero [41,50]. Likewise, the constant power load model was also used to represent the DL; further details about ELC design and control of DL can be found in studies [9–12]. In a DCIMG, the LF method utilized must account for droop Equations (1) and (2), and hence the SBFS method was proposed in [14]. This derivative-free LF method contains the following four stages.

Table 2. DG units' droop coefficients for the No DL case.

DG Unit	DG ₁	DG ₂	DG ₃	DG ₄	DG ₅	DG ₆	DG ₇	DG ₈	
m_{pi}	−0.05	−1	−0.1	−1	−0.2	−1	−0.1	−1	
n_{qi}	−0.05	−1	−0.1	−1	−0.2	−1	−0.1	−1	
Bus No.	69-bus	1	6	15	30	55	-	-	-
	118-bus	1	20	39	47	73	80	90	110

2.1.1. Initialization Stage

Since no slack bus is present in an IMG, it is replaced with a virtual bus (VB) to simulate the power exchange with a pseudo grid. Thus, in this study, Bus 1 was selected as the VB. All system voltages V_i were set to $1\angle 0^\circ$ p.u. with voltage error tolerance threshold $\varepsilon_{Th} = 10^{-8}$.

2.1.2. Backward Sweep

At this stage, all pre-islanding apparent power injects (S_i) are known, as are the bus voltages. Hence, the procedure to calculate current injects I_i followed by branch currents B_i moving backward toward the VB is as follows [14]:

$$I_i = \left(\frac{S_i}{V_i} \right)^* , \quad (3)$$

$$[B_i] = [BIBC][I_i] \quad (4)$$

where for an n bus system, $[B_i]$ and $[I_i]$ are single-column matrices of size $n - 1$ by 1 for branch and inject currents, respectively, and $[BIBC]$ is an $n - 1$ by $n - 1$ matrix for bus injection-branch current, which is filled with zeros and ones as in [51].

2.1.3. Forward Sweep

Sweeping away from VB, new voltages (V_{in}) are calculated using Equation (5). Then, the convergence criteria based on voltage error tolerance (E) is determined as in Equation (7) [14]:

$$[V_{in}] = [V_1] - [BCBV][B_i], \quad (5)$$

$$|\Delta V_{in}| = |V_{in} - V_i|, \quad (6)$$

$$E = \max \{ |\Delta V_{in}| \}, \quad (7)$$

where $[BCBV]$ is an $n - 1$ by $n - 1$ matrix for branch current and bus voltage [14].

2.1.4. The Update Stage

If the internal BFS loop converges, i.e., $E < \varepsilon_{Th}$, then deviations in frequency (Δf) and VB voltage (ΔV_1) are updated using Equations (8) and (9) as follows [14]:

$$\Delta f = -m_{pT} \cdot (P_{G1} - \Re\{V_1 \cdot B_1^*\}), \quad (8)$$

$$\Delta V_1 = -n_{qT} \cdot (Q_{G1} - \Im\{V_1 \cdot B_1^*\}), \quad (9)$$

$$f_{c_2+1} = f_{c_2} + \Delta f, \quad (10)$$

$$V_{1_{c_2+1}} = V_{1_{c_2}} + \Delta V_1, \quad (11)$$

where f_{c_2+1} and f_{c_2} are the system frequency at $c_2 + 1$ and c_2 iterations, respectively. Note that SBFS has two loops, viz., internal BFS loop with counter c_1 and external $V-f$ loop with counter c_2 ; $V_{1_{c_2+1}}$ and $V_{1_{c_2}}$ are the VB voltage at $c_2 + 1$ and c_2 iterations, respectively;

and n_{qT} and m_{pT} are the equivalent $V-f$ droop coefficients of the system, respectively, where the aggregated impact of all DGs are considered at the VB [40].

$$m_{pT} = \left(\sum_{i \in \mathcal{GK}}^{gk} m_{pi}^{-1} \right)^{-1}, \tag{12}$$

$$n_{qT} = \left(\sum_{i \in \mathcal{GK}}^{gk} n_{qi}^{-1} \right)^{-1}, \tag{13}$$

Subsequently, line impedance Z_i of branch B_i and DG powers are updated, before the final convergence check, where the algorithm terminates when $|\Delta V_1| < \epsilon_{Th}$ [14].

$$Z_i = R_i + j X_i (f_{c_2+1} / f_{c_2}), \tag{14}$$

$$P_{Gi} = \Delta f / m_{pi} + P_{Gi0}; \forall i \in \mathcal{GK}; \mathcal{GK} \subseteq \mathcal{N}, \tag{15}$$

$$Q_{Gi} = \Delta V_1 / n_{qi} + Q_{Gi0}; \forall i \in \mathcal{GK}, \tag{16}$$

where \mathcal{N} is all system buses set; \mathcal{GK} is a subset of \mathcal{N} that contains all droop buses. Likewise, system active and reactive power losses can be obtained as follows:

$$P_{loss} = \sum_{i=1}^{n-1} \Re\{Z_i\} \cdot |B_i|^2, \tag{17}$$

$$Q_{loss} = \sum_{i=1}^{n-1} \Im\{Z_i\} \cdot |B_i|^2, \tag{18}$$

The SBFS load flow method is depicted in the flow chart of Figure 3.

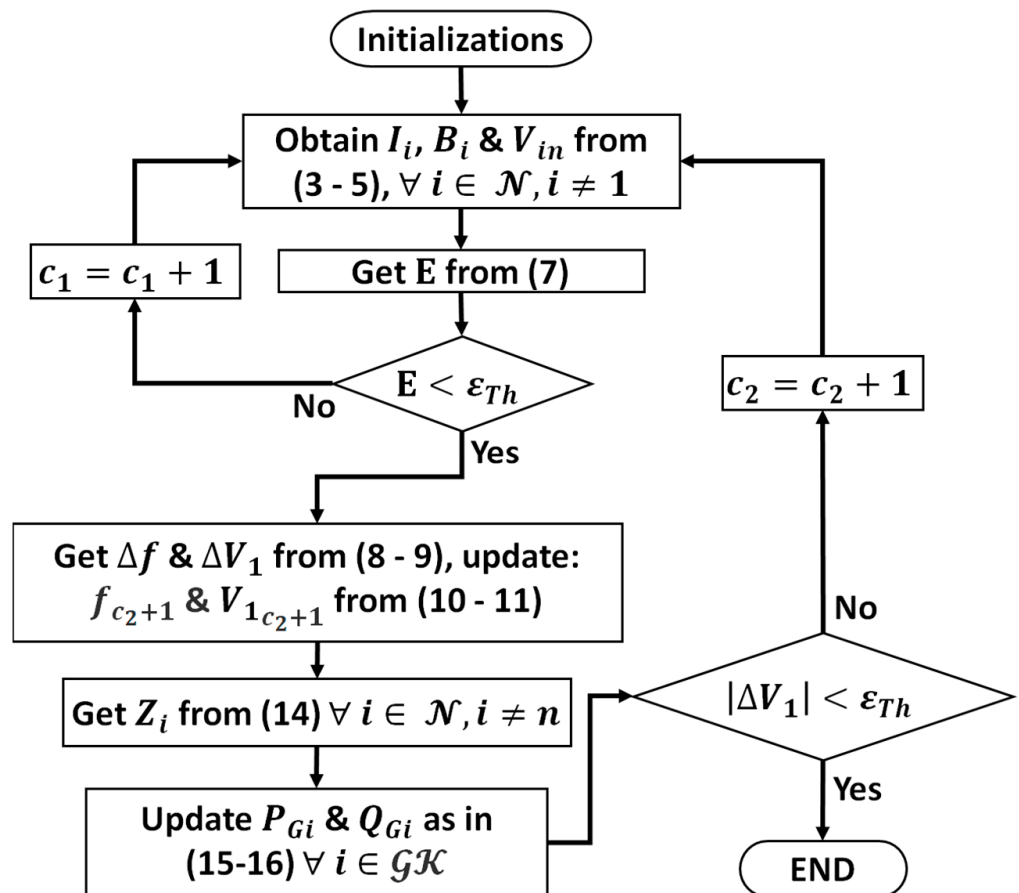


Figure 3. Special backward/forward sweep load flow method.

2.2. The Improved Special Backward/Forward Sweep (SBFS-II) Load Flow Method

In this section, the novel extension to the LF method, SBFS, as presented herein is explained. One major drawback of DBFS, which is based on global voltage updates, is having three separate loops for voltage, frequency, and BFS updates. This usually results in convergence issues for ill-conditioned problems such as the DL allocation problem addressed in this article. However, the issue was eliminated in SBFS by adopting one update loop for VB voltage and one internal loop for BFS with higher ε_{Th} . The proposed improvement to SBFS in this article, named SBFS-II, is based on Equations (5) and (7) for voltage and tolerance updates, respectively, with only one loop to update all system variables. As is the case for LF in IMG, a higher number of iterations is required to suppress the oscillations in $|\Delta V_{in}|$. However, this is not required in SBFS-II, as the reason for $|\Delta V_{in}|$ oscillations is eliminated by the removal of the BFS loop. This can be understood by examining the advantage of reactive power updates using one global voltage variable and static droop coefficients at each droop bus. Thus, the need for a voltage deviation vector across system droop buses becomes redundant. Therefore, the removal of Equation (7) by assuming $|\Delta V_{in}|$ to be zero will have a significant impact on the speed and convergence of the LF. In other words, recalculating the voltages across the system before updating the VB voltage and then doing it again after the VB update will have a negative impact on convergence and will result in more iterations required. Hence, taking the second or third guess of voltages in vector V_{in} and simultaneously calculating the VB voltage will expedite the convergence as, eventually, the required state of equilibrium is for the VB. Therefore, the voltage across the system is extended following another forward sweep to be V'_{in} , which can be obtained simply as follows:

$$I'_i = \left(\frac{S_i}{V_{in}} \right)^*, \quad (19)$$

$$[B'_i] = [BIBC][I'_i], \quad (20)$$

$$[V'_{in}] = [V_1] - [BCBV][B'_i], \quad (21)$$

where $[I'_i]$ and $[B'_i]$ are $n - 1$ -by-1 column vectors that represent the inject and branch currents following another backward sweep, observing that complex power injections and VB voltage are still constant at this stage. This is surely advantageous, as the whole focus of the LF method is in minimizing VB voltage deviation. By removing the internal BFS loop in the islanded mode, the unnecessary tolerance check for grid-connected mode by the original BFS [51] is neglected. This way, the algorithm continues to update system frequency and VB voltage based on the obtained voltages in V'_{in} . Subsequently, the change in each droop bus generation is reflected accordingly by using the obtained global variables ΔV_1 and Δf . Therefore, Equations (10) and (11) were edited to include the only remaining iteration counter (c) of SBFS-II:

$$f_{c+1} = f_c + \Delta f, \quad (22)$$

$$V_{1c+1} = V_{1c} + \Delta V_1, \quad (23)$$

Likewise, the convergence criterion in SBFS-II has also been edited to ensure that VB's power exchange is zero to avoid any conflicting results. Note that, both SBFS and SBFS-II shall give the exact same results for voltages and current injects at each bus of the system. Therefore, SBFS-II terminates when the condition for convergence is satisfied across system buses, including the VB, signaling that all generation mismatches across the system are neutralized accordingly.

$$|\Delta V'_{in}| = |V'_{in} - V_{in}|, \quad (24)$$

$$E' = |\Delta V_1| + \max\{|\Delta V'_{in}|\}, \quad (25)$$

where E' is the new voltage error tolerance across the system. A flow chart of the proposed SBFS-II is depicted in Figure 4.

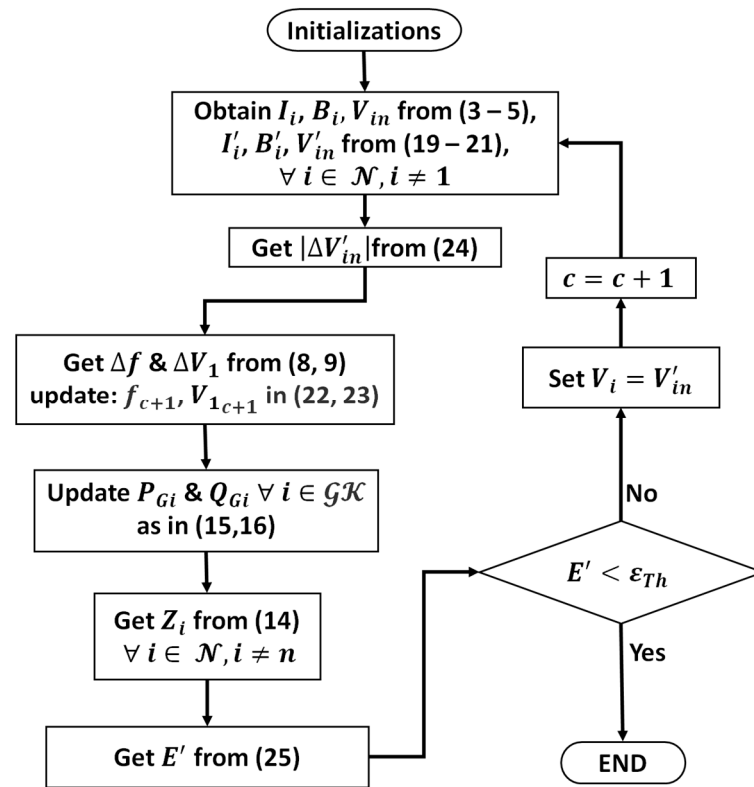


Figure 4. Improved special backward/forward sweep load flow method.

2.3. The General Backward/Forward Sweep (GBFS) Load Flow Method

The reactive power updates of SBFS and DBFS [40] are based on individual droop values of DG units and a global voltage variable ΔV_1 . This reactive power update procedure depends on the existence of adequate communication between the point of common coupling (PCC) and all DGs to spread the value of ΔV_1 to all units. However, communication in many IMGs may be limited or susceptible to delays. Therefore, an LF solution that accounts for the local voltage measurement of individual DGs, as well as their respective droops, is indeed required. On this point, a similar pattern is followed to the methods proposed in [41,42] by adopting local voltage measurement to update the reactive power. Nonetheless, the novel extension of the proposed GBFS method is the use of dynamic damping factors and reactive power correction to enhance convergence. Furthermore, similarly to SBFS-II, the proposed GBFS uses only one loop to update $\Delta V'_{in}$, Δf , ΔV_1 , and the reactive power. Moreover, MBFS [41] and NBFS [42] methods require the use of three nested loops to obtain the LF solution, viz., one for system voltages, one for VB voltage and frequency, and one for the reactive power update. However, GBFS only requires one loop to attain the system variable and complete the LF. Accordingly, the GBFS method continues by updating Equation (16) of SBFS to reflect the nominal voltage ($|V_0|$) recovery by the individual DG's reactive droop response [41,42].

$$Q_{Gi} = (|V_i| - |V_0|) / n_{qi} + Q_{Gi0}; \forall i \in \mathcal{GK}, \quad (26)$$

However, upon changing the reactive power update equation, significant convergence and stability issues were encountered. This was more evident with small values of reactive droop coefficient, higher line impedance, and the reactive power initial guess Q_{Gi0} . The issue of small droop values is of particular importance in many DCIMG optimization problems that may require smaller values of reactive droop coefficients to achieve the best possible technical and economic objectives [1,47]. To overcome convergence issues and thus minimize voltage deviations caused by lower droop values and inaccurate reactive power sharing, a dynamic damping factor, denoted as ζ_1 , is recommended. The role of ζ_1

is to suppress oscillations in the voltage update Equation (5) by minimizing the magnitude of the voltage error vector across the system $|\Delta V'_{in}|$ as follows:

$$V'_{in} = V_{in} - \zeta_1 \cdot (V_{in} - V_i), \quad (27)$$

where V'_{in} is the voltage across all system buses as obtained using ζ_1 following another forward sweep for V_i . The use of static damping factors in iterative load flow methods is a common practice in the literature [42]. Furthermore, analytical calculation of an exact value for these static damping factors is difficult and often involves trial and error to find the best value suitable to the current system state variables. However, in many LF problems in IMG, the system state variables are not constant, and hence a fixed value of damping for one problem might cause divergence in the other. In contrast, it is very difficult to analytically obtain the exact value of ζ_1 , which will result in better convergence of LF where the voltage error across the VB and the rest of system buses is minimized simultaneously [43,52]. Likewise, there are situations where load flow convergence is necessary during each function evaluation of an IMG optimization problem. Hence, attempting the trial and error of different values of the damping factor is inefficient and sometimes not possible. Moreover, due to the nature of non-linearity and non-convexity associated with most LF calculations in IMG optimization problems, metaheuristic techniques have gained popularity in finding approximate solutions by stochastic optimization [43,47]. Therefore, to ensure sufficient damping for $\Delta V'_{in}$, the value of ζ_1 is dynamically changed using the metaheuristic technique of choice such that $\Delta V'_{in}$ and VB voltage errors are minimized below the tolerance threshold ε_{Th} . There are various metaheuristic techniques available in the literature with different accuracies, speeds, programming difficulties, and calculation burdens [53]. Nonetheless, the decision on which one is more suited than the other to a specific optimization problem is open for debate. Considering all forgoing factors affecting the choice of a specific metaheuristic, speed and accuracy are the main criteria for choosing the technique adopted in GBFS. Moreover, the high-speed advantage of MIDACO algorithm makes it an appealing choice when it comes to speed and accuracy. On average, the MIDACO algorithm is up to 1500 times faster than other established evolutionary and swarm algorithms with embedded massive parallelization strategies such as the genetic algorithm [54]. Therefore, MIDACO was used to select and dynamically adjust the value of the damping factor with each iteration of the LF solution, as will be illustrated in Section 4.

To further tackle convergence problems resulting from inaccurate reactive power updates, an additional dynamic damping factor was used and is denoted as ζ_2 . The role of ζ_2 is different from ζ_1 as it was applied to VB voltage to contribute to a faster decay in ΔV_1 and enhance convergence. Unlike the static deceleration factor used in [42], ζ_1 and ζ_2 values are not constant and change by altering the LF problem states. This implies that the dynamic damping factors would have any value within a pre-defined and continuous range. On that basis, the new voltage at the VB is given by.

$$V_{1_{c+1}} = V_{1_c} + \zeta_2 \cdot \Delta V_1, \quad (28)$$

Similarly in the case of ζ_1 , it is very difficult to analytically obtain the exact value of ζ_2 that will result in better convergence of the LF where both ΔV_1 and $\Delta V'_{in}$ are minimized simultaneously. Therefore, the same approach has been adopted by dynamically changing ζ_2 until the convergence criterion is met. To ensure the best chance of convergence response, the values for ζ_1 and ζ_2 are chosen between a wide range of positive values (i.e., 0–5). Moreover, this wide range is used as the lower and upper bounds for the decision variables, which minimizes the objective function. Despite the role of ζ_1 and ζ_2 in improving the convergence of GBFS, the higher line impedance of distribution networks along with smaller droop values below certain value make accurate reactive power sharing without full communication between units a complicated task. Furthermore, the goal of most reactive power correction studies presented in [47,48], whether was based on communication between DGs, reference points setting, or virtual impedance compensation, is to equate

all reactive power update among DGs across the system. This would amount to equating reactive power error at the very last iteration of LF such that:

$$|\Delta Q_{G1}| + \gamma_1 = |\Delta Q_{G2}| + \gamma_2 = \dots = |\Delta Q_{Gi}| + \gamma_i, \quad (29)$$

where ΔQ_{Gi} is the reactive power error vector at a generating bus i , and γ_i is the reactive power correction vector needed when the updated reactive power value exceeds the limits of the DG unit. Similarly, γ_i becomes necessary when the chosen reactive droop values by the MGCC fall within a critical reactive droop range. The critical reactive droop range is defined as the range in which reactive power ceases to follow the normal linear droop relationship, where DGs start to limit power output to a min-max value or revert to constant power control. Contrariwise, in some situations, the output power may exceed the ratings of the DG leading to an IMG sequential failure, since typically all DGs are of equal rating in a DCIMG. Therefore, the introduction of γ_i to mimic the corrective control action by limiting the reactive power updates between the minimum and maximum of the DG's power rating [48,55].

$$\gamma_i = \left(\frac{Q_c}{\sum_{i \in \mathcal{GK}} |\Delta Q_{Gi}|} - 1 \right) \cdot \{|\Delta Q_{Gi}|\} \cdot \beta, \quad (30)$$

where Q_c is the average reactive-power-correction factor that could be analytically calculated by MGCC and fed to DGs with low-bandwidth communication channels. This would be equal to the mismatch at VB or the total difference in generated and consumed reactive power such that:

$$Q_c = -(Q_{G1} - \Im\{V_1 \cdot B_1^*\}), \quad (31)$$

Furthermore, the corrective effect of γ_i is based on spreading the reactive power-sharing task evenly on all DG units in the network, taking into consideration their individual reactive droop, local voltage measurement, and the residual reactive power in the system. Subsequently, editing the reference reactive power at each DG unit (Q_{Gi0}) to a value within the power ratings of the unit. This is achieved with the help of MGCC to determine the average reactive power in the system (Q_c) [48]. Based on the foregoing, the corrected Q'_{Gi0} for each DG unit becomes

$$Q'_{Gi0} = Q_{Gi0} + \gamma_i; \forall i \in \mathcal{GK}, \quad (32)$$

Subsequently, the desired reactive power generation at each droop bus is given by

$$Q'_{Gi} = Q'_{Gi0} + |\Delta Q_{Gi}|; \forall i \in \mathcal{GK}, \quad (33)$$

To ensure γ_i is used in conjunction with reactive power correction by keeping DG within their power ratings, a Boolean constant β was introduced to Equation (30). The role of β is to enable or disable the correction procedure based on the reactive power keeping requirements on a generating bus in the MG. The value of β is introduced as:

$$\beta = \begin{cases} 0, & \forall Q_{max} > Q_{Gi} > Q_{min} \\ 1, & \forall Q_{Gi} \geq Q_{max}, Q_{Gi} \leq Q_{min} \end{cases}, \quad (34)$$

where Q_{max} and Q_{min} are the maximum and minimum reactive power produced by any DG, respectively. Note that if $\beta = 0$, then the reactive power will not change, i.e., $Q'_{Gi} = Q_{Gi}$. Lastly, the proposed LF method terminates when the condition of convergence is satisfied across the system, implying that the GBFS objective function is minimized below ϵ_{Th} , as will be shown in Section 4. The general nature of the proposed LF method, GBFS, is manifested by assuming the local voltage measurements for DG units along with their respective droop values to account for the reactive power update without any communication. Moreover, simultaneously ensuring each DG does not exceed its min-max reactive power limits by adopting a correction vector in conjugation with the available communication in any IMG. Hence, the name GBFS was given to the proposed LF method, as it exhibits general

characteristics of a robust and efficient LF method in DCIMG with embedded corrective control action and communication infrastructure. The second proposed LF method, GBFS, is illustrated in the flowchart of Figure 5.

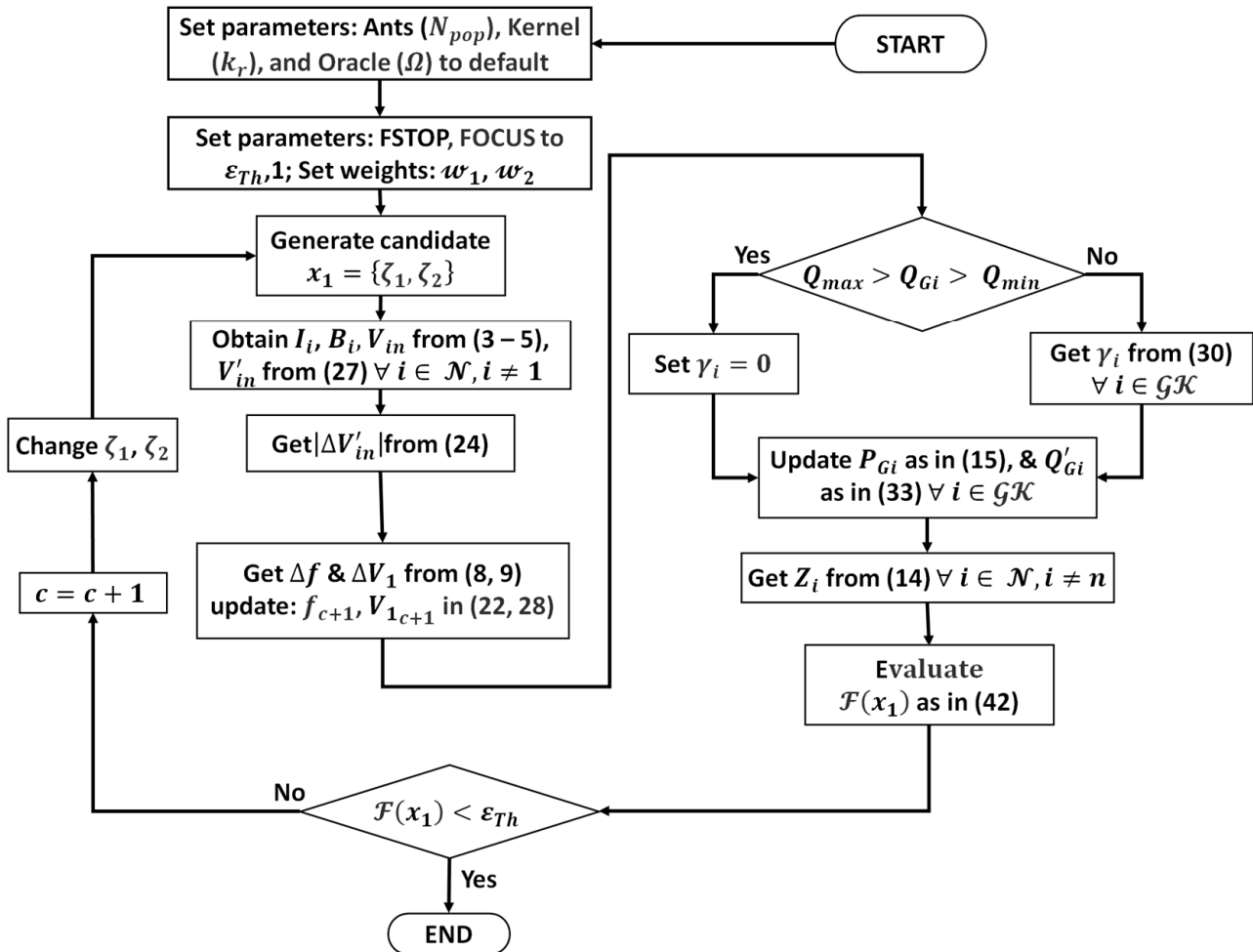


Figure 5. General backward/forward sweep load flow method.

3. The Optimization Method Proposed

The metaheuristic technique proposed in this article follows the algorithm of high-performance MIDACO. This evolutionary technique employs a black-box strategy to tackle the optimization problem. The use of metaheuristic optimization techniques is recommended if the existing deterministic solvers fail to offer solutions to real-life optimization problems. This class of problems is referred to as NP-hard problems, where analytical solutions are not available in polynomial time. Moreover, the DL allocation problem is a many-objectives non-convex mixed-integer nonlinear programming (MINLP) problem. According to the review work of [53], it was recommended that hybrid algorithms are more suited for MINLP allocation studies in microgrids. The advantage of hybrid algorithms is that they combine the exploration abilities of stochastic search and the exploitation ability of deterministic local search. Moreover, the selection of MIDACO, which is a hybridized evolutionary algorithm, makes use of an efficient back-tracking line search local solver that is pseudo gradient based [56]. Likewise, MIDACO was compared against different deterministic local solvers, wherein MIDACO was able to offer a higher number of global solutions on benchmark single-objective problems [29]. Nonetheless, the problem presented herein is a many-objective problem with huge search space, which necessitates the use of the stochastic Pareto-optimization technique to find the non-dominated solution. Inversely, the advanced multi-objective search offered by MIDACO expedites the convergence speed for

multi-objective optimization. This is attributed to the utopia-nadir information approach that guides the multi-objective search into an area of interest at the Pareto-front [27]. This is opposed to non-dominated sorting by other metaheuristics which treat the Pareto-front with equal importance, thus, adding further computation burden [56]. The inspiration for MIDACO is forged by ACOmi [25] combined with OPM for constrained problems [26]. A multi-kernel Gaussian probability density function (GPDF) is used as a probabilistic approach for the incremental building of solutions in every single objective evaluation. Unlike the original ACO, which uses pheromone tables to construct solutions, MIDACO uses GPDFs [25]. A single GPDF is not enough to focus on different promising areas of the solution search space, and hence several GPDFs of one-dimension (i) are generated in (k_r) number of kernels (\downarrow). Each GPDF has its own triplets of weight ($\mathcal{W}_{\downarrow}^i$), mean (μ_{\downarrow}^i), and standard deviation (σ_{\downarrow}^i), making the complete multi-kernel GPDF ($G^i(x)$) [23,25].

$$G^i(x) = \sum_{\downarrow=1}^{k_r} \left(\frac{\mathcal{W}_{\downarrow}^i}{\sigma_{\downarrow}^i \sqrt{2\pi}} \right) e^{-0.5 \left(\frac{x - \mu_{\downarrow}^i}{\sigma_{\downarrow}^i} \right)^2}, \quad (35)$$

In other words, the internal multi-kernel GPDF generates sufficient agents or ants (N_{pop}) in each kernel (ℓ) to obtain the objective function value and then save it, based on its importance and rank, into a solution archive (SA) [56]. For constraint handling, the oracle (Ω), a parameter associated with the universal penalty method adopted by MIDACO, can be either given by the user or estimated at a sufficiently high value to penalize any constraint violations. More details regarding the OPM can be found in [26]. To evaluate the single-objective problem, three main parameters of ACOmi, namely, N_{pop} , k_r , and Ω were incorporated in the proposed method as ANTS, KERNEL, and ORACLE parameters, respectively. For multi-objective problems, the utopia-nadir balance concept is utilized by the proposed method to fragment the original problem into single objective sub-problems to enable individual function evaluation [56]. The utopia (U_i) measures the global minimum's most superior value of a given objective function $\mathcal{F}_i(x)$ for all x solutions in the feasible domain (\mathbb{F}). Contrariwise, the nadir (N_i) is $\mathcal{F}_i(x)$'s most inferior value for all x solutions that belong to an objective function $\mathcal{F}_k(x)$ with a utopia U_k [27]:

$$U_i = \min\{\mathcal{F}_i(x) \forall x \in \mathbb{F}\}, \quad (36)$$

$$N_i = \max\{\mathcal{F}_i(x) \forall x : \exists k \neq i : \mathcal{F}_k(x) = U_k\}, \quad (37)$$

For a multi-objective problem with M objectives, several single-objective sub-problems are decomposed. Denoting $|$ for the decomposed sub-problem and \rangle for the individual objective problem, for each decomposed sub-problem with an x optimal solution, the weighted distance $d_{\rangle}^{|}(x)$ and averaged distance $D_{|}(x)$ are given as [27]

$$d_{\rangle}^{|}(x) = \frac{\mathcal{F}_{\rangle}(x) - U_{\rangle}}{N_{\rangle} - U_{\rangle}}, \quad (38)$$

$$D_{|}(x) = \frac{\sum_{\rangle=1}^M d_{\rangle}^{|}(x)}{M}, \quad (39)$$

The weighted distance of an x optimal solution for each sub-problem's utopia and nadir values defines the balance function in MIDACO [27,56].

$$B_{|}(x) = \sum_{\rangle=1}^M |d_{\rangle}^{|}(x) - D_{|}(x)|, \quad (40)$$

The balance function aims to focus the solution search efforts by the MIDACO algorithm on the Pareto front center, where the best trade-off in the multi-objective solution

exists [27,56]. The BALANCE parameter is responsible for implementing the search strategy by MIDACO considering objective ranks. Thus, the importance or insignificance of a given objective against the others is determined by a BALANCE value [56]. Furthermore, by concentrating the search efforts at a specific location on the Pareto front, the algorithm will reach the optimal solution much faster [56]. The multi-objective problem is aggregated again by solving each i -th sub-problem target function $T_i(x)$ [27].

$$T_i(x) = \sum_{j=1}^M d_j^i(x) + B_i(x), \tag{41}$$

To enhance the Pareto search efforts and calibrate the use of BALANCE, two additional parameters are used by MIDACO, namely, EPSILON and PARETOMAX [56]. The filtration precision of non-dominated solutions on the Pareto front is dictated by EPSILON, while PARETOMAX sets the maximum number of collected Pareto points. The proposed optimization method is depicted in the flow chart of Figure 6.

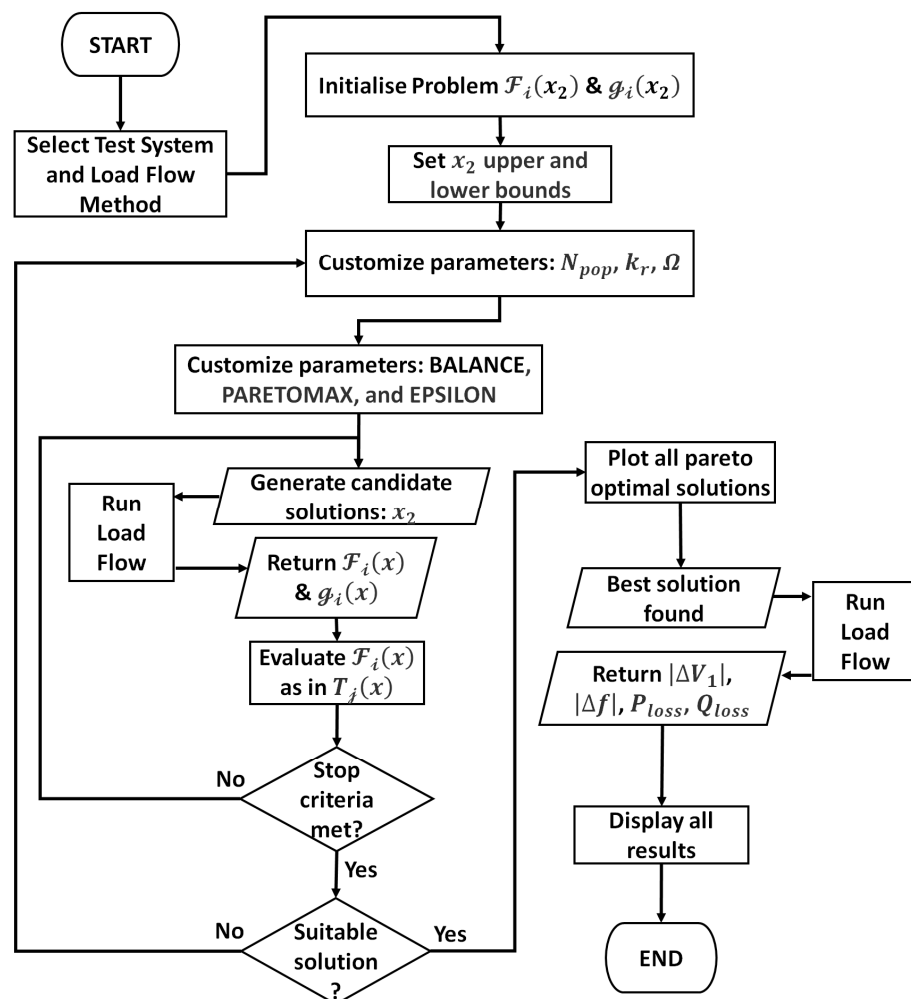


Figure 6. Proposed optimization method flow chart.

4. Optimization Problem Formulation

In this section, the proposed optimization problem is presented to determine the optimal dynamic damping factors required for GBFS convergence. Moreover, the many-objective problem for optimal DL sizing and location as well as the optimal droop selection for DG are elucidated in more detail.

4.1. General Backward/Forward Sweep Optimization Problem

In this subsection, the optimization problem formulation for the proposed GBFS method is presented in detail.

4.1.1. Objective Function

The aim of the GBFS optimization problem is to attain the simultaneous minimization of the voltage error across system buses ($|\Delta V'_{in}|$) and the voltage error at the virtual bus ($|\Delta V_1|$). The significance of these two voltage deviation errors is fundamental for the convergence of the load-flow solution. This is attributed to their influence as they guarantee the satisfaction of power mismatch across system buses. When the values for ζ_1 and ζ_2 dynamically change, the oscillations in $|\Delta V'_{in}|$ and $|\Delta V_1|$ are damped, respectively. Thus, an enhanced convergence response of LF is achieved by keeping the voltage error below a tolerance threshold value, i.e., ε_{Th} . To obtain the desired objective function in GBFS with minimal evaluation time, a weighted sum approach was adopted. The use of a weighted sum to transform the multi-objective problem into a single objective simplifies the optimization problem and enhances the calculation speed. This can be easily understood since pre-knowledge of the maximum threshold for a desired objective function value, which in this case is equal to ε_{Th} , makes the search for an optimal value below that threshold a relatively simple task. This is opposed to the standard need for exploration and exploitation by metaheuristics to know what the global optima look like. This criterion is easily implemented in MIDACO by the simple tuning of the parameters FOCUS and FSTOP. Accordingly, FOCUS steers the solution search space towards a local region where the desired objective threshold value lies, while FSTOP halts the algorithm as soon as the value of the objective function falls below the specified threshold [56]. The advantage of MIDACO's deterministic local search is better utilized when the area of solution search space is reduced around the current optimal solution. The use of the FOCUS parameter, which is one of the most advanced parameters in hybrid evolutionary computation, expedite the local search convergence of the internal deterministic solver in MIDACO [56]. This is very beneficial in significantly reducing the computational burden for the proposed GBFS. Moreover, despite the multi-objective capability of MIDACO, the use of a weighted sum approach against Pareto-front techniques is well known to significantly expedite the speed of individual function evaluation, that is, if speed was desired over accuracy [47,53]. The objective function presented in GBFS is given as follows:

$$\mathcal{F}(x_1) = \varpi_1 \cdot \max\{|\Delta V'_{in}|\} + \varpi_2 \cdot |\Delta V_1|, \quad (42)$$

$$x_1 = \{\zeta_1, \zeta_2\}, \quad (43)$$

$$0 < \zeta_1 \leq 5, \quad (44)$$

$$0 < \zeta_2 \leq 5, \quad (45)$$

where ϖ_1 and ϖ_2 are weights for $|\Delta V'_{in}|$ and $|\Delta V_1|$, and equal 1 and 1, respectively; $\mathcal{F}(x_1)$ is the GBFS objective function corresponding to a decision variable x_1 . Note that the x_1 range and $\{\varpi_1, \varpi_2\}$ are editable from problem to problem for enhanced convergence.

4.1.2. Constraints

The use of constraints in the GBFS optimization problem is not necessary since the objective is merely to select ζ_1 and ζ_2 that minimizes the objective $\mathcal{F}(x_1)$ below ε_{Th} . Moreover, frequency, bus voltage, and line limits are often associated with the main optimization study and do not interfere with GBFS's purpose of providing a converged LF solution regardless of operational system limits. Therefore, to further enhance the speed, the constraint handling function of MIDACO, $\mathcal{C}(x_1)$ was set to zero.

4.2. Dump-Load-Allocation Optimization Problem

In this subsection, the many-objectives optimization problem investigated for DL allocation in DCIMG is presented in detail.

4.2.1. Objective Functions

The motivation behind DL allocation to minimize $V-f$ deviations relates back to previous DL use as a heating and pumping application [57,58]. Nonetheless, previous DL attempts were targeted at a generating bus without reference to operation at off-peak hours. Moreover, power losses were considered as drawbacks for DL use with generating units. However, in this study, DL allocation is random for any bus in the system satisfying certain criteria such as minimal power loss. The many-objectives problem of DL allocation as tackled herein aims to find an optimal DL location and size with optimal droop gains for optimal DG dispatch. The MINLP problem is formulated to minimize all four objectives simultaneously via the Pareto optimization technique. The four objectives are voltage deviations ($|\Delta V_1|$), frequency deviations ($|\Delta f|$), active (P_{loss}), and reactive (Q_{loss}) power losses. The first two objectives are based on Equations (8) and (9) for voltage and frequency deviations, respectively. Note that the method to calculate $V-f$ as the aggregated effect of all DG units at the virtual bus is the same for each LF technique discussed herein. Similarly, the last two objectives are calculated using Equations (17) and (18) for active and reactive losses, respectively. Moreover, the exploration by the optimization technique, MIDACO, was enhanced with the two newly proposed LF methods (i.e., SBFS-II and GBFS). This shall result in an improved DL allocation by enhancing the solution search space and expand the solvable region. Thus, the many-objectives function $\mathcal{F}_\gamma(x_2)$ and the decision variable x_2 are formulated as follows:

$$\mathcal{F}_\gamma(x_2) = \min\{|\Delta V_1|, |\Delta f|, P_{loss}, Q_{loss}\}, \quad (46)$$

$$x_2 = \{P_{DL}, Q_{DL}, mn_{DL}, N_{DL}\}, \quad (47)$$

where P_{DL} and Q_{DL} are the active and reactive powers for the DL, respectively; N_{DL} is the DL bus number; and mn_{DL} is the droop value for the DL allocation, which has been selected such that $mn_{DL} = m_{pi} = n_{qi}, \forall i \in \mathcal{GK}$ [14]. The value of mn_{DL} is seen as the optimal value for DG dispatch to minimize power losses upon the inclusion of DL into the microgrid [14]. According to the many-objectives problem given in $\mathcal{F}_\gamma(x_2)$, the proposed optimization technique will fragment the problem into a set of many single-objective sub-problems [27]. Subsequently, the set of sub-problems for each objective will be aggregated into a target function to be minimized based on the utopia-nadir information. Each individual sub-problem is evaluated as an individual ACOmi instance in a massive parallelization framework [27]. With each generation of ACOmi instances, the subproblems exchange the utopia, nadir, and best-known solution information with each other. This is important for multi-objective convergence, as it will prevent clustering at edges or specific areas of the Pareto front [27]. It is worth noting that the focus in $V-f$ objectives aimed to minimize the first step of Figure 2. This is attributed to their high percentage of total $V-f$ deviations compared to other droop steps. This is of particular importance for $V-f$ deviation minimization, as the remaining steps typically approach zero upon the convergence of LF. In other words, minimizing the influential initial droop step will implicitly keep all expected $V-f$ deviations at droop buses to a minimum.

4.2.2. Constraints

According to international standards for islanded systems such as IEEE 1547.4 [59] and international standards for DG interconnection such as IEEE 1547.7 [49], certain technical requirements must be adhered in islanded system operation. This implies that frequency, bus voltage, and line thermal limits must be adequate to ensure stable islanding operation.

Therefore, the many-objectives problem presented in this article was subjected to constraint function (i.e., $\{x_2\}$) as given below,

$$\{x_2\} = \{|V_i|, |B_i|, f, P_{DG}, Q_{DG}\}, \forall i \in \mathcal{N}, \tag{48}$$

with the operational limits defined as follows:

Bus voltage limits [2]

$$0.95 \leq |V_i| \leq 1.05, \tag{49}$$

Thermal limits below maximum branch current (B_{i_max}).

$$|B_i| \leq |B_{i_max}|, \tag{50}$$

A min–max limit for all DG units [14].

$$0 \leq P_{DG} \leq 2, \tag{51}$$

$$0 \leq Q_{DG} \leq 2, \tag{52}$$

An operating system frequency limit [2].

$$0.996 \leq f \leq 1.004, \tag{53}$$

Moreover, the decision variable x_2 had the following limits:

DL size limits [14].

$$0.002 \leq P_{DL} \leq 1, \tag{54}$$

$$0.002 \leq Q_{DL} \leq 1, \tag{55}$$

Drop coefficient value limits [14].

$$10^{-4} \leq mn_{DL} \leq 1, \tag{56}$$

Note that the nominal frequency was $f_0 = 50$ Hz, while all given values were in p.u. at the system base of 500 kVA for both test systems. Furthermore, a nominal voltage of 12.66 kV and 11 kV were assumed for the 69- and 118-bus systems, respectively.

5. Discussion of Results

The autonomous microgrids investigated in this article are the benchmark test systems of IEEE 69- and 118-bus systems as depicted in Figure 7.

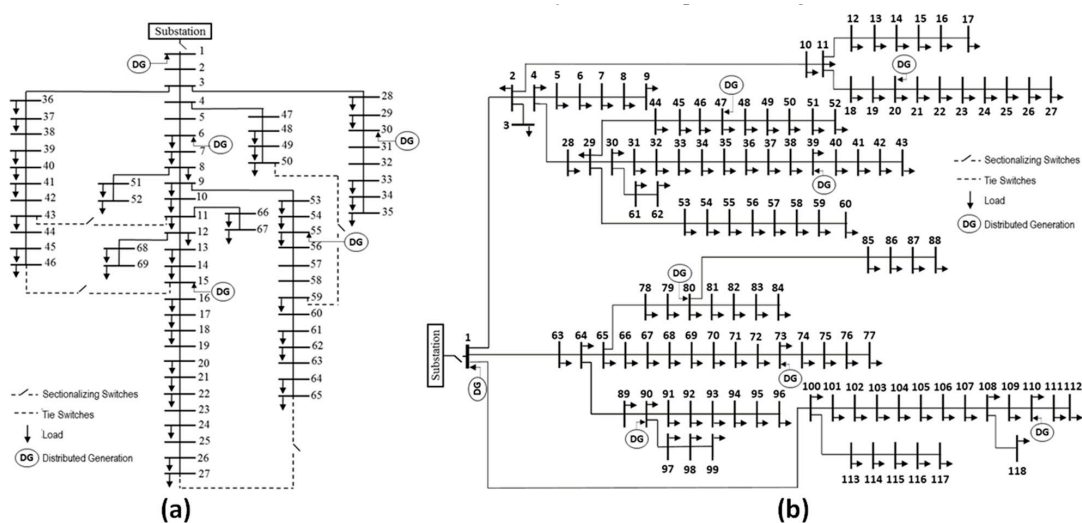


Figure 7. Modified microgrid single line diagram: (a) IEEE 69-bus; (b) IEEE 118-bus.

System data were adopted from [60] for the 69- and 118-bus systems. Moreover, the two systems had identical DG units connected to buses given in Table 2 and depicted in Figure 7. The pre-islanding generation was $0.9 + j0.9$ p.u. and $1.52 + j1.52$ p.u. for the 69- and 118-bus systems, respectively. Generation/loading scenario is given in Table 3 for both test systems [14]. The use of normal distribution for load uncertainty is a common practice in the literature [20,61], while values close to the mean have the highest probability of occurrence in a normal distribution. Hence, for the sake of brevity, the generation/loading scenario centered around the mean during off-peak hours was adopted, since it was sufficient to simulate a high probable mismatch occurrence in a DCIMG [61].

Table 3. Test system generation to load states for 69- and 118-bus systems.

Test System	Load (%)	ΣP_{Li} (p.u.)	ΣQ_{Li} (p.u.)	Generation (%)	ΣP_{Gi} (p.u.)	ΣQ_{Gi} (p.u.)	Mismatch (%)
69	100	7.6044	5.3892	100	8	6	+7.29
	50	3.8022	2.6946	63.63	4.5	4.5	+36.56
118	100	45.42	34.08	100	43.24	32.43	-4.82
	50	22.71	17.04	63.63	24.32	24.32	+21.14

5.1. Significance of the Damping Factors ζ_1 and ζ_2

To understand the significance of the proposed two dynamic damping factors and their influence on the LF solution for DCIMG, a six-bus IMG was depicted in Figure 8.

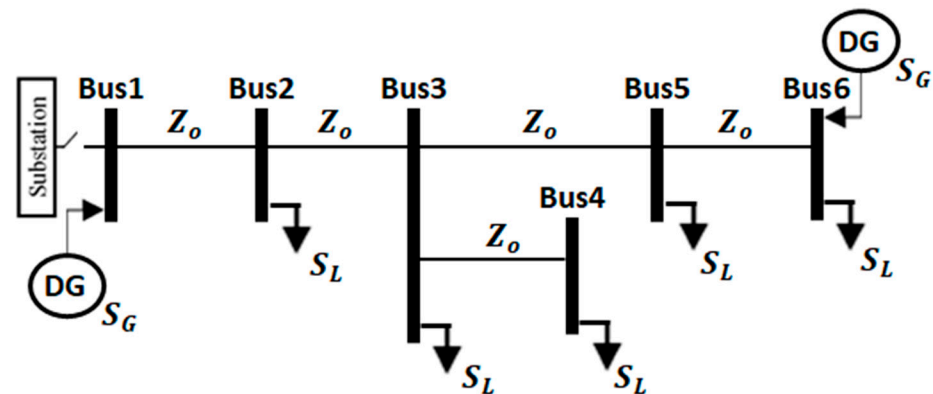


Figure 8. Six-bus microgrid.

The system data were adopted from [62], with a 11 kV and 500 kVA system base. To demonstrate the impact of dynamic damping factors, the system was assumed to have identical loads across all buses except the VB, i.e., bus 1. Thus, loads were selected such that $S_L = 0.6 + j0.3$ p.u. [62], while two identical DGs were installed at buses 1 and 6, respectively, with pre-islanding generation $S_G = 2 + j0.75$ p.u. Furthermore, three variations for the 6-bus system's line impedance (Z_o) and reactive droops (n_{qo}) were considered to imitate the ill-conditioning expected in IMG with radial topology [63].

This shall increase the complexity of finding a converged LF solution using the three LF methods, namely, MBFS, NBFS, and the proposed method GBFS. The six-bus system was subjected to five convergence tests using variations in line impedance and droop settings as given in Table 4 [63].

Subsequently, the load flow analysis results considering test 1 for the three LF methods, viz., MBFS, NBFS, and GBFS, are given in Table 5. According to the LF results in Table 5, all three methods managed to attain the exact same values for voltage magnitudes and angles, while both DGs reported the same active and reactive power generation output. Nonetheless, GBFS had the fastest calculation time, followed by NBFS and then MBFS.

Table 4. Line impedance and droop sets for the six-bus system.

Test	1	2	3	4	5
R_o (Ω)	0.19	1.10	1.64	0.19	0.19
L_o (mH)	1.96	3.20	4.53	1.96	1.96
m_{p_o} (p.u.)	9.51×10^{-3}	9.51×10^{-3}	9.51×10^{-3}	4.52×10^{-3}	3.53×10^{-3}
n_{q_o} (p.u.)	1.83×10^{-2}	1.83×10^{-2}	1.83×10^{-2}	8.94×10^{-3}	5.89×10^{-3}

R_o and L_o are resistance and inductance of branches with impedance Z_o , respectively; m_{p_o} and n_{q_o} are active and reactive droops for DGs in the six-bus system.

Table 5. Load flow analysis results for the six-bus system considering test 1 of Table 4.

Bus No.	Bus Voltage (p.u.)			Voltage Angle (degree $^\circ$)		
	MBFS	NBFS	GBFS	MBFS	NBFS	GBFS
1	1.0008	1.0008	1.0008	0	0	0
2	0.9979	0.9979	0.9979	-0.1901	-0.1901	-0.1901
3	0.9961	0.9961	0.9961	-0.3057	-0.3057	-0.3057
4	0.9949	0.9949	0.9949	-0.3814	-0.3814	-0.3814
5	0.9969	0.9969	0.9969	-0.2702	-0.2702	-0.2702
6	0.9989	0.9989	0.9989	-0.1596	-0.1596	-0.1596
MVE	0.0051	0.0051	0.0051	-	-	-

Bus No.	DG Active Power (p.u.)			DG Reactive Power (p.u.)		
	MBFS	NBFS	GBFS	MBFS	NBFS	GBFS
1	1.5021	1.5021	1.5021	0.7046	0.7046	0.7046
6	1.5021	1.5021	1.5021	0.8092	0.8092	0.8092

	Active Power Losses (p.u.)			Reactive Power Losses (p.u.)		
	MBFS	NBFS	GBFS	MBFS	NBFS	GBFS
value	0.0042	0.0042	0.0042	0.0138	0.0138	0.0138

	Frequency (p.u.)			Calculation Time (s)		
	MBFS	NBFS	GBFS	MBFS	NBFS	GBFS
value	1.0047	1.0047	1.0047	0.0133	0.0083	0.0004

Similarly, the convergence advantage of GBFS over MBFS and NBFS is given in Table 6. As can be seen from Table 6, using a lower reactive droop setting has negatively impacted the reactive power updates in MBFS and NBFS, making LF convergence not possible. On the contrary, GBFS has managed to obtain a converged LF solution within a reasonable number of iterations. This is due to ζ_1 and ζ_2 and their influence on $|\Delta V'_{in}|$ and $|\Delta V_1|$ damping. Likewise, in the case of altering the line impedance, i.e. changing the R/X ratio, convergence issues were also observed with MBFS and NBFS, as they failed to converge for both test 2 and test 3.

Table 6. Number of load flow iterations for the six-bus system considering tests of Table 4.

Convergence Test	Load Flow Method				
	MBFS	NBFS	GBFS		
				Iterations	ζ_1
1	422	283	6	0.6257	0.7146
2	NC	NC	13	4.9676	1.2926
3	NC	NC	20	2.6396	1.5002
4	NC	NC	12	4.6345	1.2639
5	NC	NC	50	3.7655	1.7974

NC: Not Converged.

On the other hand, the sensitivity of the LF solution to the damping factors was demonstrated by altering the optimal value of damping to see its impact on LF solution convergence, and results are given in Table 7. As can be deduced from the results, convergence tolerance to the value of ζ_2 was much lower than it was for ζ_1 . This was evident

upon the divergence caused in GBFS due to a very slight change in optimal ζ_2 value, while relatively larger deviations in ζ_1 did not significantly impact the convergence of GBFS.

Table 7. Sensitivity of load flow solution to the values of ζ_1 and ζ_2 for the six-bus system.

Test 1	ζ_1	6.26×10^{-7}	6.26×10^{-3} *	0.6257 *	6.6257	12.626	21.626
	Iterations	7	7	6	9	11	15
	ζ_2	7.15×10^{-4}	0.0715	0.7146 *	1.6146	2.0146	2.5146
	Iterations	NC	183	7	62	NC	NC
Test 3	ζ_1	6.4×10^{-3}	0.6396	2.6396 *	3.6396	5.6396	6.6396
	Iterations	34	31	20	52	308	NC
	ζ_2	0.9002	1.2002	1.5002 *	1.9002	2.2002	2.5002
	Iterations	NC	453	20	110	NC	NC
Test 5	ζ_1	7.7×10^{-3}	1.7655	3.7655 *	4.7655	5.7655	7.1566
	Iterations	68	57	50	91	213	NC
	ζ_2	1.1974	1.4974	1.7974 *	2.0974	2.3974	2.6974
	Iterations	NC	NC	50	NC	NC	NC

NC: Not Converged, * indicates the optimal value for the damping factor.

5.2. Multi-Objective Optimization

The multi-objective optimization problem, as given in (46) earlier, was tackled using the two newly developed load flow methods embedded within MIDACO. To simulate the multi-objective problem using MIDACO, the parameters PARETOMAX, EPSILON, and BALANCE were set to 1000, 0.01, and 0, respectively. Similarly, the default values selected for ANTS, KERNEL, and ORACLE were 0, 0, and 10^9 , respectively. Conversely, to initialize the optimization problem within the GBFS method, the parameters FOCUS and FSTOP were initialized accordingly.

FOCUS was two and three for the 69- and 118-bus systems, respectively, while FSTOP was set to 10^{-8} for both test systems. Moreover, the mismatch scenario of Table 3 was used to simulate the over-generation state in the IMG for both test systems. The multi-objective results are given in Tables 8 and 9 for the 69- and 118-bus systems, respectively. Accordingly, the obtained LF solution using SBFS-II for the base case (i.e., using droop settings of Table 2 without DL in the system) was identical for both test systems if compared to the SBFS solution.

Additionally, the DL allocation results using the SBFS-II method for both test systems were very similar to the ones previously obtained by SBFS in [14]. This slight change in DL values did not have any notable impact on the accuracy of the obtained values for the four objectives. On the contrary, the calculation time improved by adopting SBFS-II as the LF method. As given in Table 8, the calculation time for the 69-bus systems was 38 s using SBFS-II compared to 43 s for the SBFS method, whereas, as given in Table 9, the calculation time of the 118-bus system improved by 8 s using SBFS-II. This running time improvement can be attributed to the shorter duration needed for an individual function evaluation instance by the removal of the internal BFS loop in SBFS-II. Therefore, adopting SBFS-II in the optimization algorithm of MIDACO notably improved the calculation time without impacting the accuracy of the original optimization method using SBFS.

On the other hand, adopting the GBFS method in the optimization algorithm of MIDACO significantly improved the values for all four objective functions. As given in Tables 8 and 9, the obtained $|\Delta V_1|$ values were significantly smaller compared to those obtained by SBFS and SBFS-II. While the obtained values for $|\Delta f|$ by GBFS were slightly lower than those of the other two LF methods. This behavior can be explained by the significant improvement GBFS brought to the LF solution by providing more accurate reactive power updates based on the local voltage measurement by all DGs and their respective

droop values. Inversely, in SBFS and SBFS-II, the reactive power-update mechanism is dependent on the global variable $|\Delta V_1|$, which neglects the effect of line impedance and local DG terminal voltage.

Table 8. Multi-objective results with different load flow methods for the 69-bus system.

Load Flow Method	SBFS		SBFS-II		GBFS	
	No DL	With DL	No DL	With DL	No DL	With DL
N_{DL}	-	30	-	30	-	30
P_{DL} (p.u.)	-	0.6580	-	0.6551	-	0.6282
Q_{DL} (p.u.)	-	0.5135	-	0.5246	-	0.8000
mn_{DL} (p.u.)	-	0.0487	-	0.0489	-	0.0102
$ \Delta V_1 $ (p.u.)	0.0480	0.0123	0.0480	0.0123	0.0480	0.0020
$ \Delta f $ (p.u.)	0.0170	0.0003	0.0170	0.0002	0.0171	0.0000
P_{loss} (p.u.)	0.0578	0.0617	0.0578	0.0617	0.0577	0.0606
Q_{loss} (p.u.)	0.0251	0.0255	0.0251	0.0255	0.0250	0.0251
MVE (p.u.)	0.0500	0.0188	0.0500	0.0188	0.0503	0.0290
f_{ss} (p.u.)	1.0173	0.9998	1.0173	0.9998	1.0173	1.0000
Calculation Time (s)	-	43	-	38	-	50

MVE : maximum voltage error, f_{ss} : steady-state frequency, $|\Delta V_1|$ and $|\Delta f|$ are for first step size only.

Table 9. Multi-objective results with different load flow methods for the 118-bus system.

Load Flow Method	SBFS		SBFS-II		GBFS	
	No DL	With DL	No DL	With DL	No DL	With DL
N_{DL}	-	73	-	73	-	80
P_{DL} (p.u.)	-	0.4771	-	0.5073	-	0.9996
Q_{DL} (p.u.)	-	0.7289	-	0.6658	-	0.8461
mn_{DL} (p.u.)	-	0.0117	-	0.0117	-	0.0083
$ \Delta V_1 $ (p.u.)	0.1454	0.0094	0.1454	0.0095	0.1453	0.0066
$ \Delta f $ (p.u.)	0.0281	0.0014	0.0281	0.0013	0.0281	0.0004
P_{loss} (p.u.)	0.1335	0.1157	0.1335	0.1157	0.1316	0.1065
Q_{loss} (p.u.)	0.0908	0.0779	0.0908	0.0779	0.0893	0.0712
MVE (p.u.)	0.1636	0.0218	0.1636	0.0219	0.1607	0.0125
f_{ss} (p.u.)	1.0301	1.0015	1.0301	1.0014	1.0302	1.0005
Calculation Time (s)	-	62	-	54	-	100

Results of $|\Delta V_1|$ and $|\Delta f|$ are for the first step size only.

Likewise, the obtained active and reactive power losses by GBFS were improved compared to those of SBFS and SBFS-II. This improvement in loss objectives can also be realized by the advantage of local reactive power updates based on local DG bus voltage in GBFS rather than reactive power updates based on one global bus voltage (the voltage at the VB in our case studies). In other words, the difference between the total generated power by each DG unit post-islanding and the total network demand including DL was reduced according to the solution obtained by GBFS. This reduction was achieved even though the new DL value obtained by GBFS was higher than that of SBFS and SBFS-II. However, the new DL resulted in greatly reduced branch currents for both bus systems.

Inversely, the non-dominated solution for both test systems considering all three load flow methods is depicted in Figure 9.

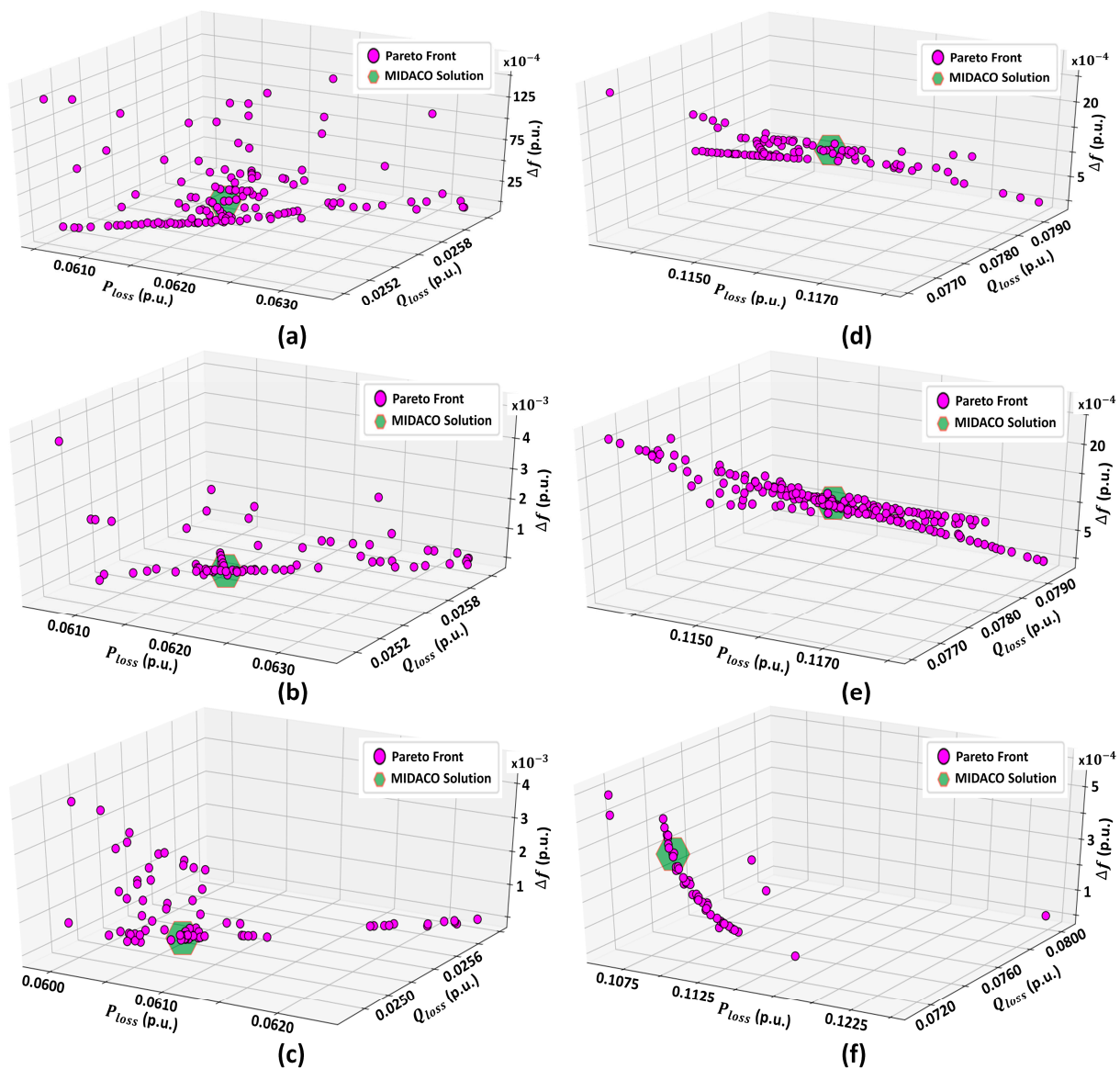


Figure 9. Many-objectives Pareto front considering different load-flow methods; the optimal solution is highlighted with the green shape for (a) SBFS in 69-bus, (b) SBFS-II in 69-bus, (c) GBFS in 69-bus, (d) SBFS in 118-bus, (e) SBFS-II in 118-bus, and (f) GBFS in 118-bus.

According to Figure 9, the resultant Pareto front shape did not significantly change considering SBFS or SBFS-II for both test systems. Nonetheless, adopting the GBFS method in the optimization algorithm did in fact alter the shape and number of non-dominated solutions. It is noteworthy that the default value of the BALANCE parameter did not change for any of the cases in Figure 9, nor did the default values for EPSILON and PARETOMAX. However, the Pareto front shape and the number of non-dominated solutions are also problem specific the same as they are influenced by the latter parameters. Furthermore, when GBFS was used, the problem's solution search space shrank compared to the SBFS and SBFS-II solution domains. This is due to the limited number of lower droop values that guarantee a converged solution in GBFS, which does not constitute an issue with SBFS and SBFS-II, as they are global voltage based-LF methods.

Lastly, to highlight the advancements in the solution to the DL allocation problem, the solution obtained by MIDACO with the SBFS technique was compared with the solutions attained by the two proposed LF techniques. The improvements against the SBFS solution

are given in Table 10 as the percentage difference from original SBFS solution. The negative percentage indicates a reduction (i.e., improvement) in the original value.

Table 10. Percentage difference in the multi-objective results for both test systems.

Solution Method	SBFS/MIDACO		SBFS-II/MIDACO		GBFS/MIDACO	
Test System	69	118	69	118	69	118
$ \Delta V_1 $ (%)	-	-	0	+1.06	-83.74	-29.79
$ \Delta f $ (%)	-	-	-33.33	-7.14	-100	-71.43
P_{loss} (%)	-	-	0	0	-1.78	-7.95
Q_{loss} (%)	-	-	0	0	-1.57	-8.6
Calculation Time (%)	-	-	-11.63	-12.9	+16.28	+61.29

5.3. Comparison with Other Metaheuristic Methods

The advantage of the proposed optimization method using GBFS was compared with other metaheuristic techniques, viz., multi-objective GA (MOGA), multi-objective PSO (MOPSO), and NSGA-II [64]. The results obtained by each of the three metaheuristics using GBFS as the LF method are given in Table 11 for both test systems.

Table 11. Comparison of the multi-objective problem's solution with other metaheuristics.

Metaheuristic	MOGA		NSGA-II		MOPSO		MIDACO	
Bus System	69	118	69	118	69	118	69	118
N_{DL}	30	80	30	80	30	80	30	80
P_{DL} (p.u.)	0.8544	0.4203	0.6877	0.9720	0.7228	0.7096	0.6282	0.9996
Q_{DL} (p.u.)	0.5556	0.9540	0.4768	0.9800	0.5454	0.5628	0.8000	0.8461
mn_{DL} (p.u.)	0.0543	0.0084	0.0511	0.0088	0.0488	0.0086	0.0102	0.0083
$ \Delta V_1 $ (p.u.)	0.0133	0.0065	0.0133	0.0068	0.0120	0.0071	0.0020	0.0066
$ \Delta f $ (p.u.)	0.0024	0.0010	0.0006	0.0005	0.0009	0.0007	0.0000	0.0004
P_{loss} (p.u.)	0.0607	0.1077	0.0606	0.1065	0.0607	0.1066	0.0606	0.1065
Q_{loss} (p.u.)	0.0250	0.0716	0.0251	0.0713	0.0251	0.0712	0.0251	0.0712
MAXEVAL	400	400	200	200	500	500	10000	10000
Time ^a (s)	4564	5223	8479	9811	4587	5870	50	100

Results of $|\Delta V_1|$ and $|\Delta f|$ are for first step size only; ^a algorithm computation time.

Tests were carried out using the generation/demand state in Table 3, while the parameter setup for the other metaheuristics was based on [64]. The selected parameters for MOGA were 100, 0.8, and 0.001 for population size, crossover, and mutation probabilities, respectively. Furthermore, MOPSO parameters were as follows: number of grids per dimension was 7; repository and population size were 100; coefficients of social and cognitive learning were 0.2 and 0.1, respectively; pressures of leader and deletion selection were 2; rates of inflation and mutation were 0.1; and weights for inertia starting and ending were 0.5 and 0.001, respectively. Lastly, NSGA-II had four parameters in total: population size was 100, crossover and mutation distribution indexes were 100 and 20, respectively, and the mutation probability was 0.25. As given in Table 11, the obtained losses by all methods were close for both test systems, except for MOGA, as active losses were higher overall. Contrariwise, the first two objectives by MIDACO were significantly lower than the rest of the methods. Lastly, the clear speed advantage by MIDACO was demonstrated by obtaining thousands of function evaluations with very low time compared to the other methods. This significant time and accuracy advantage of the proposed optimization method shall enable real-time application with the shortest possible optimization cycle.

5.4. Convergence of SBFS-II and GBFS Methods

To further validate the two proposed LF methods' efficacy in finding a converged LF solution within finite number of iterations, three convergence tests were considered whose details are given in Table 12. The convergence curves of ΔV_1 over 100 iterations for all investigated LF methods on the 69- and 118-bus systems are illustrated in Figure 10. From the latter figure, the SBFS-II method holds the best convergence response for all investigated convergence tests for both bus systems, while GBFS has better response compared to its counter parts MBFS and NBFS.

Table 12. Load flow calculation times in seconds for both test systems.

Convergence Test		1		2		3	
Description		Base Case (No DL) ^a		w/DL Using GBFS Solution		w/DL Using Random Guess ^b	
Test System		69	118	69	118	69	118
mn_{DL}		-	-	0.0102	0.0083	0.0075	0.0093
P_{DL} (p.u.)		-	-	0.6282	0.9996	0.0043	0.0034
Q_{DL} (p.u.)		-	-	0.8000	0.8461	0.0051	0.0075
Load Flow Method & Time (s)	DBFS	0.0461	NC	NC	NC	NC	NC
	SBFS	0.0080	0.0103	0.0070	0.0085	0.0066	0.0092
	SBFS-II	0.0054	0.0070	0.0042	0.0055	0.0038	0.0058
	MBFS	0.0238	0.0421	NC	NC	NC	NC
	NBFS	0.0219	0.0400	NC	NC	NC	NC
	GBFS	0.0085	0.0126	0.0096	0.0461	0.0116	0.0248

^a Using droop values from Table 2; ^b randomly generated solution within the first 100 evaluations by MIDACO; NC: Not Converged.

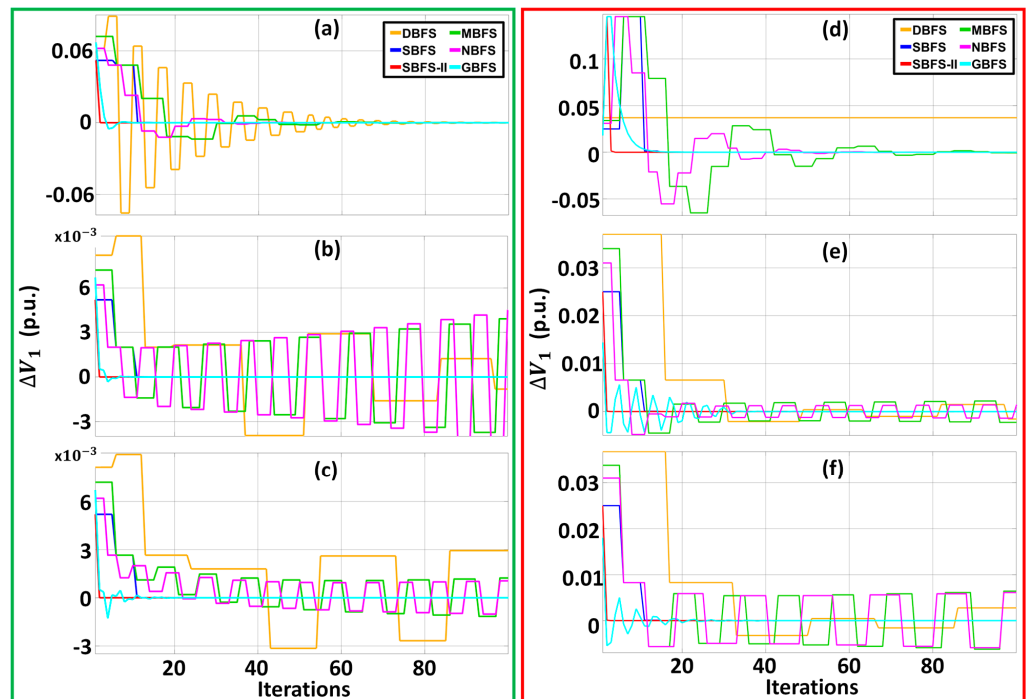


Figure 10. Convergence tests of ΔV_1 for (a) Test 1—69-bus, (b) Test 2—69-bus, (c) Test 3—69-bus, (d) Test 1—118-bus, (e) Test 2—118-bus, and (f) Test 3—118-bus.

On the other hand, the advancements in calculation times using SBFS-II and GBFS were compared against the SBFS, DBFS, MBFS, and NBFS methods using the same convergence tests of Table 12. The resulting calculation times are given in Table 12 for both bus systems. As can be seen from Table 12, SBFS-II has the fastest calculation time among all available LF methods, while the calculation times of SBFS and GBFS are the second and third best. The reason behind the speed of the SBFS methods over the other local voltage measurement methods such as GBFS, MBFS, and NBFS is attributed to the influence of the global voltage variable distributed among all DGs. This influence is realized by an expedited convergence process by dictating the same rate of reactive power update between DG units in the system. Furthermore, the superior performance of GBFS against MBFS and NBFS, which are all LF methods based on local voltage measurements, comes from adopting two dynamic damping factors and the reactive power correction vector, which enhances the convergence of the LF solution without compromising the accuracy of the solution.

6. Conclusions

In this article, the optimization problem of DL allocation using the MIDACO algorithm with two newly developed LF methods, i.e., SBFS-II and GBFS, was addressed. The optimization problem was formulated to minimize $V-f$ deviations and network power losses during off-peak hours within the DCIMG framework. The SBFS-II method uses a global voltage value spread to all generating units with one computational loop to suppress oscillations in $|\Delta V'_{in}|$. On the other hand, the GBFS method utilization of two dynamic damping factors minimizes the oscillations in $|\Delta V'_{in}|$ and $|\Delta V_1|$ simultaneously using the high-speed metaheuristic MIDACO. The significance of GBFS's damping factors was demonstrated on a six-bus system using variations of line impedance and reactive droops. Additionally, GBFS employs a reactive power correction vector to limit power updates by DGs within their min–max limits. The advantage of DL allocation in DCIMG using MIDACO with the two LF methods was validated on the 69- and 118-bus systems. The attained results demonstrate a better convergence response for SBFS-II with faster calculation times compared to the former method SBFS. This was reflected in the results with 11.63% and 12.9% reductions in the calculation times for the 69- and 118-bus systems, respectively. Conversely, GBFS's results provided higher accuracy compared to those of SBFS without a significant reduction in calculation speeds for the DL allocation problem. Taking the frequency deviation results, this amounted to a reduction of 100% and 71.43% in the objective function value for the 69- and 118-bus system, respectively. Furthermore, the efficacy of results produced by the proposed optimization method was compared with other metaheuristic methods. In the end, the reported results of the two LF methods as combined with MIDACO herein should provide further significance to the advantage of DL allocation in IMG with high penetration levels. Similarly, the proposed LF methods should serve as helpful tools in future planning and optimization studies of DCIMG. That is, based on practical and communication limitations, GBFS could be sought over SBFS-II. Future work in this article could be expanded to account for the load flow of meshed topology and unbalanced islanded distribution networks. Furthermore, the allocation of the DL problem could be expanded to account for uncertainty in generation and demand forecast as well as DL use for heating applications.

Author Contributions: Conceptualization, M.Z.K. and A.F.Z.; methodology, M.Z.K. and A.F.Z.; investigation, M.Z.K.; writing—original draft preparation, M.Z.K.; writing—review and editing, A.F.Z.; supervision, A.F.Z. All authors have read and agreed to the published version of the manuscript.

Funding: This research received no external funding.

Data Availability Statement: The data supporting the reported results are available in the manuscript.

Acknowledgments: Funds were received from Brunel University London for covering the costs for open access publishing.

Conflicts of Interest: The authors declare no conflict of interest.

Appendix A

Table A1. List of symbols and nomenclatures.

Symbol	Definition	Symbol	Definition
$V-f$	Voltage and frequency	$V_{1_{c+1}}, V_{1_c}$	Virtual bus voltage at the $c_2 + 1$ and c_2 iterations within SBFS-II and GBFS framework
f, f_0, f_{ss}	Operational, nominal, and steady-state frequency, respectively	$\Delta V'_{in}$	The deviation in voltage error across the system within SBFS-II and GBFS framework
V_i, V_0	Operational and nominal voltage at bus i , respectively	E'	Voltage error tolerance for SBFS-II convergence
P_{Gi0}, P_{Gi}	Bus i 's active nominal and generated power, respectively	ε_{Th}	Tolerance threshold for load flow convergence
Q_{Gi0}, Q_{Gi}	Bus i 's reactive nominal and generated power, respectively	Q_{min}, Q_{max}	Minimum and maximum reactive power output of DG, respectively
m_{pi}, n_{qi}	Bus i 's droop coefficients for frequency and voltage, respectively	ΔQ_{Gi}	Reactive power update error at bus i
m_{pT}, n_{qT}	Frequency and voltage equivalent droop coefficients, respectively	Q_c	Average reactive power correction factor
mn_{DL}	Dump load allocation's optimum droop settings for DGs	Q'_{Gi0}, Q'_{Gi}	Adjusted reference and desired reactive power at bus i , respectively
N_{DL}	Dump load bus location	ζ_1, ζ_2	Dynamic damping factors
P_{DL}, Q_{DL}	The dump load's consumed active and reactive power, respectively	\exists_1, \exists_2	Weights for GBFS objective function
gk	Total number of dispatchable DGs in the IMG	x_1	GBFS optimization problem decision variable
\mathcal{N}	All system buses set	$\mathcal{F}(x_1)$	GBFS optimization problem objective function
\mathcal{GK}	A subset containing all dispatchable DG buses	γ_i	Reactive power correction vector
P_{loss}, Q_{loss}	The MG's total losses for active and reactive power, respectively	β	A binary constant to enable reactive power correction
$\Delta V_1, \Delta f$	Virtual bus voltage and frequency deviations, respectively	U_j, N_j	The objective function's utopia and nadir values, respectively
S_i, I_i	Injections of apparent power and current at bus i within the SBFS framework, respectively	$\mathcal{F}_j(x)$	The optimization problem's objective function within the MIDACO framework
B_i	The current flowing in the branch between bus i to bus $i + 1$	$\mathcal{J}_i(x)$	The constraints handling function within the MIDACO framework
V_{in}	New bus voltage following forward sweep within SBFS framework	$G^i(\mathcal{S})$	Multi-dimensional Gaussian function
ΔV_{in}	The deviation in voltage error across the system within the SBFS framework	$\mathcal{W}_{\downarrow}^i, \mu_{\downarrow}^i, \sigma_{\downarrow}^i$	Weight, mean, and standard deviation for the Gaussian function, respectively
f_{c_2+1}, f_{c_2}	Frequency at the $c_2 + 1$ and c_2 iterations within the SBFS framework, respectively	x	The optimization problem's decision variable within the MIDACO framework
$V_{1_{c_2+1}}, V_{1_{c_2}}$	Virtual bus voltage at the $c_2 + 1$ and c_2 iterations within the SBFS framework, respectively	w_j^i	Each sub-problem's matrix of weights
Z_i, R_i, X_i	Impedance, resistance, and reactance of branch B_i , respectively	$d_j^i(x), D_j(x)$	Solution x weighted and average distances, respectively
E	Voltage error tolerance for SBFS convergence	$B_j(x), T_j(x)$	The balance and target functions, respectively
$[B'_i], [I'_i]$	The inject and branch currents following another backward sweep, respectively	x_2	Decision variable within dump load allocation problem
$[V'_{in}]$	The voltage column vector across the system following another sweep	$\mathcal{F}_j(x_2)$	Objective function for dump load allocation problem
f_{c+1}, f_c	Frequency at the $c + 1$ and c iterations within SBFS-II and GBFS framework	$\mathcal{J}_j(x_2)$	Constraint function for dump load allocation problem

References

1. Anderson, A.; Suryanarayanan, S. Review of energy management and planning of islanded microgrids. *CSEE J. Power Energy Systems* **2020**, *6*, 329–343. [[CrossRef](#)]
2. *IEEE Std 1547–2018*; IEEE Standard for Interconnection and Interoperability of Distributed Energy Resources with Associated Electric Power Systems. Interfaces Revision of IEEE Std 1547–2003; IEEE: New York, NY, USA, 2018; pp. 1–138. [[CrossRef](#)]
3. Guerrero, M.; Vasquez, J.; Matas, J.; de Vicuna, L.; Castilla, M. Hierarchical Control of Droop-Controlled AC and DC Microgrids—A General Approach Toward Standardization. *IEEE Trans. Ind. Electron.* **2011**, *58*, 158–172. [[CrossRef](#)]
4. Nisar, A.; Thomas, M.S. Comprehensive Control for Microgrid Autonomous Operation with Demand Response. *IEEE Trans. Smart Grid* **2017**, *8*, 2081–2089. [[CrossRef](#)]
5. Chen, S.; Zhang, T.; Gooi, H.; Masiello, R.; Katzenstein, W. Penetration Rate and Effectiveness Studies of Aggregated. BESS for Frequency Regulation. *IEEE Trans. Smart Grid* **2016**, *7*, 167–177. [[CrossRef](#)]
6. Singh, S.; Jagota, S.; Singh, M. Energy management and voltage stabilization in an islanded microgrid through an electric vehicle charging station. *Sustain. Cities Soc.* **2018**, *41*, 679–694. [[CrossRef](#)]
7. Faisal, M.; Hannan, M.; Ker, P.; Hussain, A.; Mansor, M.; Blaabjerg, F. Review of Energy Storage System Technologies in Microgrid Applications: Issues and Challenges. *IEEE Access* **2018**, *6*, 35143–35164. [[CrossRef](#)]
8. Haidar, A.M.A.; Muttaqi, K.; Sutanto, D. Technical challenges for electric power industries due to grid-integrated electric vehicles in low voltage distributions: A review. *Energy Convers. Manag.* **2014**, *86*, 689–700. [[CrossRef](#)]
9. Roodsari, B.N.; Nowicki, E.; Freere, P. A New Electronic Load Controller for the Self-excited Induction Generator to Decrease Stator Winding Stress. *Energy Procedia* **2014**, *57*, 1455–1464. [[CrossRef](#)]
10. Singh, R.R.; Kumar, B.; Shruthi, D.; Panda, R.; Raj, C.T. Review and experimental illustrations of electronic load controller used in standalone Micro-Hydro generating plants. *Eng. Sci. Technol. Int. J.* **2018**, *21*, 886–900. [[CrossRef](#)]
11. Mufaris, A.L.M.; Baba, J. Coordinated Consumer Load Control by Use of Heat Pump Water Heaters for Voltage Rise Mitigation in Future Distribution System. In Proceedings of the 7th IEEE AGTC, New Orleans, LA, USA, 15–17 April 2015; pp. 176–182. [[CrossRef](#)]
12. Nehrir, M.H.; Lameres, B.; Venkataramanan, G.; Gerez, V.; Alvarado, L.A. An approach to evaluate the general performance of stand-alone wind/photovoltaic generating systems. *IEEE Trans. Energy Convers.* **2000**, *15*, 433–439. [[CrossRef](#)]
13. Uniyal, A.; Sarangi, S.; Kala, H. Optimal dump load allocation to regulate voltage and frequency in microgrid. In Proceedings of the 8th ICPS, Jaipur, India, 20–22 December 2019; pp. 1–6. [[CrossRef](#)]
14. Kreishan, M.Z.; Zobia, A.F. Allocation of Dump Load in Islanded Microgrid Using the Mixed-Integer Distributed Ant Colony Optimization. *IEEE Syst. J.* **2022**, *16*, 2568–2579. [[CrossRef](#)]
15. Awad, A.S.A.; EL-Fouly, T.; Salama, M.M.A. Optimal ESS Allocation and Load Shedding for Improving Distribution System Reliability. *IEEE Trans. Smart Grid* **2014**, *5*, 2339–2349. [[CrossRef](#)]
16. Mukhopadhyay, B.; Das, D. Optimal multi-objective expansion planning of a droop-regulated islanded microgrid. *Energy* **2021**, *218*, 119415. [[CrossRef](#)]
17. Džamarija, M.; Keane, A. Autonomous Curtailment Control in Distributed Generation Planning. *IEEE Trans. Smart Grid* **2016**, *7*, 1337–1345. [[CrossRef](#)]
18. Gupta, Y.; Nellikkath, R.; Chatterjee, K.; Doolla, S. Volt-var Optimization and Reconfiguration: Reducing Power Demand and Losses in a Droop-Based Microgrid. *IEEE Trans. Ind. Appl.* **2021**, *7*, 2769–2781. [[CrossRef](#)]
19. Dheer, D.K.; Soni, N.; Doolla, S. Improvement of small signal stability margin and transient response in inverter-dominated microgrids. *Sustain. Energy Grids Netw.* **2016**, *5*, 135–147. [[CrossRef](#)]
20. Jithendranath, J.; Das, D. Scenario-based multi-objective optimisation with loadability in islanded microgrids considering load and renewable generation uncertainties. *IET Renew. Power Gener.* **2019**, *13*, 785–800. [[CrossRef](#)]
21. Abdelaziz, M.M.A.; Farag, H.; El-Saadany, E.F. Optimum Reconfiguration of Droop-Controlled Islanded Microgrids. *IEEE Trans. Power Syst.* **2016**, *31*, 2144–2153. [[CrossRef](#)]
22. Dorigo, M.; Caro, G.; Gambardella, L.M. Ant Algorithms for Discrete Optimization. *Artif. Life* **1999**, *5*, 137–172. [[CrossRef](#)]
23. Socha, K.; Dorigo, M. Ant colony optimization for continuous domains. *Eur. J. Oper. Res.* **2008**, *185*, 1155–1173. [[CrossRef](#)]
24. Lopez-Ibanez, M.; Stutzle, T. The Automatic Design of Multiobjective Ant Colony Optimization Algorithms. *IEEE Trans. Evol. Comput.* **2012**, *16*, 861–875. [[CrossRef](#)]
25. Schlüter, M.; Egea, J.; Banga, J.R. Extended ant colony optimization for non-convex mixed integer nonlinear programming. *Comput. Oper. Res.* **2009**, *36*, 2217–2229. [[CrossRef](#)]
26. Schlüter, M.; Gerdt, M. The oracle penalty method. *J. Glob. Optim.* **2010**, *47*, 293–325. [[CrossRef](#)]
27. Schlueter, M.; Yam, C.; Watanabe, T.; Oyama, A. Many-objective optimization of interplanetary space mission trajectories. In Proceedings of the IEEE CEC, Sendai, Japan, 25–28 May 2015; pp. 3256–3262. [[CrossRef](#)]
28. Schlueter, M. MIDACO software performance on interplanetary trajectory benchmarks. *Adv. Space Res.* **2014**, *54*, 744–754. [[CrossRef](#)]
29. Schlüter, M.; Gerdt, M.; Rückmann, J.J. A numerical study of MIDACO on 100 MINLP benchmarks. *Optimization* **2012**, *61*, 873–900. [[CrossRef](#)]
30. Shirmohammadi, D.; Hong, H.; Semlyen, A.; Luo, G.X. A compensation-based power flow method for weakly meshed distribution and transmission networks. *IEEE Trans. Power Syst.* **1988**, *3*, 753–762. [[CrossRef](#)]

31. Luo, G.X.; Semlyen, A. Efficient load flow for large weakly meshed networks. *IEEE Trans. Power Syst.* **1990**, *5*, 1309–1316. [[CrossRef](#)]
32. Dukpa, A.; Venkatesh, B.; El-Hawary, M. Application of continuation power flow method in radial distribution systems. *Electr. Power Syst. Res.* **2009**, *79*, 1503–1510. [[CrossRef](#)]
33. Bompard, E.; Carpaneto, E.; Chicco, G.; Napoli, R. Convergence of the backward/forward sweep method for the load-flow analysis of radial distribution systems. *Int. J. Electr. Power Energy Syst.* **2000**, *22*, 521–530. [[CrossRef](#)]
34. Abdelaziz, M.M.A.; Farag, H.; El-Saadany, E.; Mohamed, Y.A.I. A Novel and Generalized Three-Phase Power Flow Algorithm for Islanded Microgrids Using a Newton Trust Region Method. *IEEE Trans. Power Syst.* **2013**, *28*, 190–201. [[CrossRef](#)]
35. Nazari, A.A.; Keyypour, R.; Beiranvand, M.; Amjady, N. A decoupled extended power flow analysis based on Newton-Raphson method for islanded microgrids. *Int. J. Electr. Power Energy Syst.* **2020**, *117*, 105705. [[CrossRef](#)]
36. Bayat, M.; Koushki, M.; Ghadimi, A.; Tostado-Véliz, M.; Jurado, F. Comprehensive enhanced Newton Raphson approach for power flow analysis in droop-controlled islanded AC microgrids. *Int. J. Electr. Power Energy Syst.* **2022**, *143*, 108493. [[CrossRef](#)]
37. Mumtaz, F.; Syed, M.H.; Hosani, M.A.; Zeineldin, H.H. A Novel Approach to Solve Power Flow for Islanded Microgrids Using Modified Newton Raphson with Droop Control of DG. *IEEE Trans. Sustain. Energy* **2016**, *7*, 493–503. [[CrossRef](#)]
38. Lisboa, A.C.; Guedes, L.; Vieira, D.; Saldanha, R.R. A fast power flow method for radial networks with linear storage and no matrix inversions. *Int. J. Electr. Power Energy Syst.* **2014**, *63*, 901–907. [[CrossRef](#)]
39. Petridis, S.; Blanas, O.; Rakopoulos, D.; Stergiopoulos, F.; Nikolopoulos, N.; Voutetakis, S. An Efficient Backward/Forward Sweep Algorithm for Power Flow Analysis through a Novel Tree-Like Structure for Unbalanced Distribution Networks. *Energies* **2021**, *14*, 897. [[CrossRef](#)]
40. Díaz, G.; Gómez-Aleixandre, J.; Coto, J. Direct Backward/Forward Sweep Algorithm for Solving Load Power Flows in AC Droop-Regulated Microgrids. *IEEE Trans. Smart Grid* **2016**, *7*, 2208–2217. [[CrossRef](#)]
41. Hameed, F.; Al Hosani, M.; Zeineldin, H.H. A Modified Backward/Forward Sweep Load Flow Method for Islanded Radial Microgrids. *IEEE Trans. Smart Grid* **2019**, *10*, 910–918. [[CrossRef](#)]
42. Kumar, A.; Jha, B.; Dheer, D.; Singh, D.; Misra, R.K. Nested backward/forward sweep algorithm for power flow analysis of droop regulated islanded microgrids. *Transm. Distrib. IET Gener.* **2019**, *13*, 3086–3095. [[CrossRef](#)]
43. Elrayah, A.; Sozer, Y.; Elbuluk, M.E. A Novel Load-Flow Analysis for Stable and Optimized Microgrid Operation. *IEEE Trans. Power Deliv.* **2014**, *29*, 1709–1717. [[CrossRef](#)]
44. Esmaeli, A.; Abedini, M.; Moradi, M.H. A novel power flow analysis in an islanded renewable microgrid. *Renew. Energy* **2016**, *96*, 914–927. [[CrossRef](#)]
45. Reddy, Y.O.; Jithendranath, J.; Chakraborty, A.K.; Guerrero, J.M. Stochastic optimal power flow in islanded DC microgrids with correlated load and solar PV uncertainties. *Appl. Energy* **2022**, *307*, 118090. [[CrossRef](#)]
46. Fotopoulou, M.; Petridis, S.; Karachalios, I.; Rakopoulos, D. A Review on Distribution System State Estimation Algorithms. *Appl. Sci.* **2022**, *12*, 11073. [[CrossRef](#)]
47. Kreishan, M.Z.; Zobia, A.F. Optimal Allocation and Operation of Droop-Controlled Islanded Microgrids: A Review. *Energies* **2021**, *14*, 4653. [[CrossRef](#)]
48. Han, Y.; Li, H.; Shen, P.; Coelho, E.; Guerrero, J.M. Review of Active and Reactive Power Sharing Strategies in Hierarchical Controlled Microgrids. *IEEE Trans. Power Electron.* **2017**, *32*, 2427–2451. [[CrossRef](#)]
49. *IEEE Std 1547.7-2013*; IEEE Guide for Conducting Distribution Impact Studies for Distributed Resource Interconnection. IEEE: New York, NY, USA, 2014; pp. 1–137. [[CrossRef](#)]
50. Li, Y.; Chiang, H.-D.; Choi, B.K.; Chen, Y.T.; Huang, D.H.; Lauby, M.G. Load models for modeling dynamic behaviors of reactive loads: Evaluation and comparison. *Int. J. Electr. Power Energy Syst.* **2008**, *30*, 497–503. [[CrossRef](#)]
51. Teng, J.H. A direct approach for distribution system load flow solutions. *IEEE Trans. Power Deliv.* **2003**, *18*, 882–887. [[CrossRef](#)]
52. He, J.; Li, Y.W. An Enhanced Microgrid Load Demand Sharing Strategy. *IEEE Trans. Power Electron.* **2012**, *27*, 3984–3995. [[CrossRef](#)]
53. Pesaran, M.; Huy, P.D.; Ramachandramurthy, V.K. A review of the optimal allocation of distributed generation: Objectives, constraints, methods, and algorithms. *Renew. Sustain. Energy Rev.* **2017**, *75*, 293–312. [[CrossRef](#)]
54. Schlueter, M.; Munetomo, M. Parallelization strategies for evolutionary algorithms for MINLP. In Proceedings of the IEEE CEC, Cancun, Mexico, 20–23 June 2013; pp. 635–641. [[CrossRef](#)]
55. Zhu, Y.; Zhuo, F.; Shi, H. Accurate power sharing strategy for complex microgrid based on droop control method. In Proceedings of the IEEE ECCE Asia Downunder, Melbourne, VIC, Australia, 3–6 June 2013; pp. 344–350. [[CrossRef](#)]
56. MIDACO-SOLVER, MIDACO_User_Manual. Available online: http://www.midaco-solver.com/data/other/MIDACO_User_Manual.pdf (accessed on 21 June 2022).
57. Bhakar, P.S.; Rao, G.; Sarangi, S. A Novel Adaptive Frequency Control Strategy for Micro Grid. In Proceedings of the 14th IEEE INDICON, Roorkee, India, 15–17 December 2017; pp. 1013–1018. [[CrossRef](#)]
58. Tomar, A.; Sharma, D.; Mishra, S. An active power management strategy in a microgrid having static and rotating generators considering generation limits using water pumping loads. In Proceedings of the ICCCE, Jaipur, India, 1–2 July 2017; pp. 484–488. [[CrossRef](#)]
59. *IEEE Std 1547.4-2011*; IEEE Guide for Design, Operation, and Integration of Distributed Resource Island Systems with Electric Power Systems. IEEE: New York, NY, USA, 2011; pp. 1–54. [[CrossRef](#)]

60. Saha, S.; Mukherjee, V. Optimal placement and sizing of DGs in RDS using chaos embedded SOS algorithm. *IET Gener. Transm. Distrib.* **2016**, *10*, 3671–3680. [[CrossRef](#)]
61. Niknam, T.; Kavousifard, A.; Aghaei, J. Scenario-based multiobjective distribution feeder reconfiguration considering wind power using adaptive modified particle swarm optimization. *IET Renew. Power Gener.* **2012**, *6*, 236–247. [[CrossRef](#)]
62. Au, M.T.; Milanovic, J.V. Development of Stochastic Aggregate Harmonic Load Model Based on Field Measurements. *IEEE Trans. Power Deliv.* **2007**, *22*, 323–330. [[CrossRef](#)]
63. Mahdavi, M.; Alhelou, H.H.; Cuffe, P. Test Distribution Systems: Network Parameters and Diagrams of Electrical Structural. *IEEE Open Access J. Power Energy* **2021**, *8*, 409–420. [[CrossRef](#)]
64. Zobaa, A.F. Mixed-Integer Distributed Ant Colony Multi-Objective Optimization of Single-Tuned Passive Harmonic Filter Parameters. *IEEE Access* **2019**, *7*, 44862–44870. [[CrossRef](#)]

Disclaimer/Publisher’s Note: The statements, opinions and data contained in all publications are solely those of the individual author(s) and contributor(s) and not of MDPI and/or the editor(s). MDPI and/or the editor(s) disclaim responsibility for any injury to people or property resulting from any ideas, methods, instructions or products referred to in the content.